ON THE USE OF A JANUS-INSPIRED DATA FRAME TO ESTIMATE CHANNEL CHARACTERISTICS FOR ADAPTIVE COMMUNICATION SYSTEMS

by

Ananya Bhattacharya

Submitted in partial fulfillment of the requirements
for the degree of Master of Applied Science

at

Dalhousie University
Halifax, Nova Scotia
November 2023

To my loving family and a friend, whose unwavering support, encouragement, and sacrifices have been instrumental in my journey.

Table of Contents

List of Tables

List of Figures

Abstract

The JANUS protocol is being used widely in underwater acoustic sensor networks for various applications including but not limited to mammal habitat monitoring, event detection, submarine communication and surveillance due to their reliability. JANUS was designed with error correction techniques and robust modulation schemes to make them immune to the harsh channel conditions. In this thesis, a broadcast message that incorporates various features of the JANUS standard is designed to obtain an average estimate of the channel impairments in an underwater communication link. The discovered channel parameters such as signal-to-noise ratio (SNR), channel impulse response (CIR), Doppler shift, Doppler spread, and RMS delay spread can be effectively utilized to define the transmission parameters for a reconfigurable physical layer for an underwater communication network. The thesis describes the algorithms used to estimate the gain, multipath properties and Doppler spread within the channel. These algorithms are then demonstrated over a simulated data as well as on a measured data-set for a communication link with a bandwidth of 5 kHz at 27.5 kHz. The estimated channel data provides valuable information for estimating the achievable throughput in a channel, considering factors such as the number of subcarriers and modulation ratio. Conversely, for a desired throughput, the estimated channel data can also be used to determine the optimal number of subcarriers for a multi-carrier modulation system.

Acknowledgements

I would like to express my heartfelt gratitude to my supervisor, Dr. Jean-François Bousquet, for his invaluable guidance, unwavering support, and immense expertise throughout my thesis journey. Dr. Bousquet's deep knowledge of the subject matter, insightful feedback, and constant encouragement have been instrumental in shaping the direction and quality of my research. His mentorship has not only enhanced my technical skills but also nurtured my growth as a researcher.

I would like to thank the entire crew of HMCS Kingston for supporting the sea-trial as well as Defence RD Canada- Atlantic Research Centre personnel, particularly Alan Polvi, Mark Baldin, Val Shepeta, Gordon Murray, and Mike Simms.

I am also deeply grateful to the members of the UW-Stream research team for their continuous assistance, support, and motivation. Their willingness to share their knowledge, brainstorm ideas, and provide valuable input has played a crucial role in the success of my thesis. Their collaborative spirit and dedication to excellence have fostered an environment of creativity and intellectual growth that greatly enriched my research experience.

I would also like to extend my appreciation to the members of the Electrical and Computer Engineering department at Dalhousie University. Their organization of insightful seminars and provision of essential resources have been immensely helpful in my thesis writing process. The department's commitment to fostering a vibrant research community and providing a conducive learning environment has been instrumental in my personal and academic development.

Lastly, I would like to express my gratitude to my family, friends, and loved ones for their unwavering support, understanding, and encouragement throughout this challenging yet rewarding journey. Their belief in my abilities, words of encouragement, and patience have been a constant source of motivation, enabling me to overcome obstacles and stay focused on my goals.

I am truly grateful to all those who have contributed to my thesis, directly or indirectly, and whose support has been invaluable. Their collective efforts have made this research endeavor possible and have shaped my academic journey.

Chapter 1

Introduction

1.1 Background

The ocean is an incredible resource that covers more than 70 percent of the planet's surface. It is home to a tremendous amount of biodiversity that plays a critical role in supporting diverse ecosystems and regulating the earth's temperature. The oceans are a major source of food and transportation, currently contributing to 2.5% of global gross domestic product (GDP) [1]. However, due to factors like over-exploration, pollution, unsustainable fishing practices, climate change and marine habitat destruction, our oceans face several threats such as balance disruption in the marine food webs, oxygen depletion due to nutrient run-off, ocean acidification, coral bleaching and catastrophic decline in marine species and habitats [2], [3].

In contrast to terrestrial wireless communications which rely on electromagnetic energy, underwater communication is best achieved through acoustic propagation rather than Radio Frequency (RF) signals. Research studies, such as the work by Steele et al. [4], have emphasized the superiority of acoustic communication in underwater environments due to the ability to travel significantly larger distances in water compared to RF signals, making them ideal for long-range communication. The high density and compressibility of water provides an efficient medium for sound propagation, allowing acoustic waves to maintain their integrity over extended distances with minimal loss. In contrast, RF signals experience severe attenuation, absorption, and signal loss when transmitted underwater, whereas optical signals, though unaffected by attenuation, undergoes scattering thereby necessitating high precision laser beams, rendering them impractical for reliable long-distance communication.

The origins of underwater acoustic communication may be traced back to the early twentieth century [5], when primitive underwater telegraphy systems based on sound signals and Morse code were established. During World War II, the need for underwater communication systems was recognized for submarine combat and anti-submarine operations, which led to

developments in hydrophones, transducers, and sonar devices for communication and detection. Underwater telephone systems came into existence in the mid-twentieth century, facilitating voice communication underwater. Analog systems advanced simultaneously, boosting communication and underwater detection capabilities. Digital signal processing techniques became common as technology advanced, resulting in enhanced data rates and reliability in underwater communication systems. Today, with the advent of the smart ocean concept and the Internet of Underwater Things (IoUT), underwater communication networks with heterogeneous sensor nodes demand a wide variety of requirements for throughput, range and reliability [6].

A flow diagram representing an underwater acoustic transceiver to enable bi-directional communication is shown in Figure 1.1. The transmitter block in an underwater acoustic communication system employs channel encoding to add bit redundancy for error correction. The encoded data is modulated using a carrier frequency and converted to a passband signal. A digital-to-analog converter (DAC) is implemented to enable transmission across the underwater acoustic channel. To counter additive noise, the signal is pre-amplified and then passed through a power amplifier for enhanced signal power. The digital signal is then transmitted across the underwater acoustic channel after being emitted by transducer hydrophones.

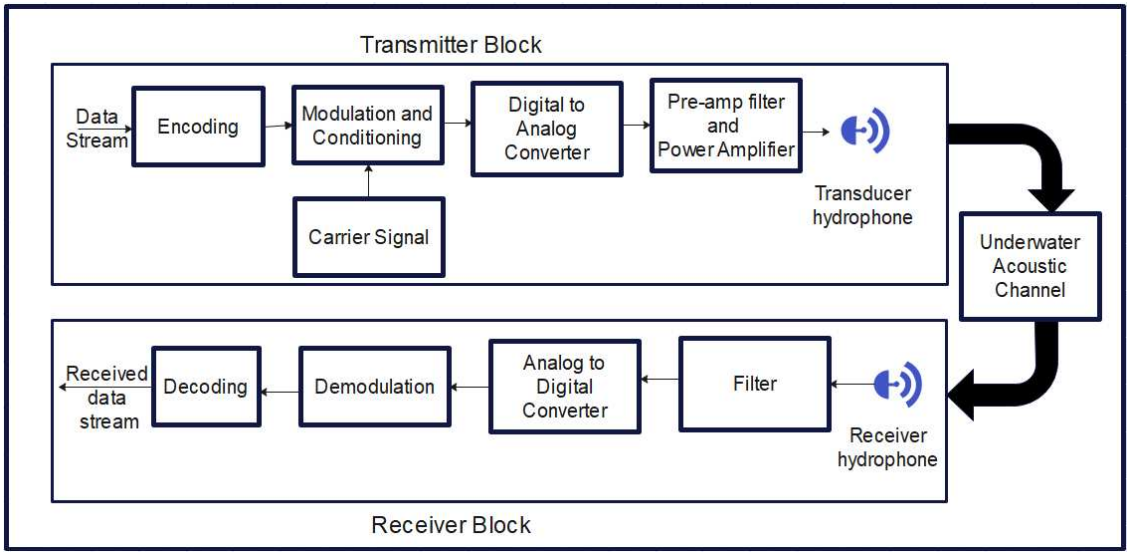

Figure 1.1: Block Diagram of a the physical layer for an underwater acoustic transceiver

At the receiver end, the hydrophones intercept the signal transmitted through the channel. The received signal undergoes filtering to remove additive noise and is converted back to

its analog form. Subsequently, the signal is demodulated and downconverted to its baseband frequency. Finally, channel decoding is applied to retrieve the original data stream from the signal.

Figure 1.2 is a representation of a typical deployment in a shallow water conditions. An instrument is moored at the bottom and a second instrument is fixed onto a mobile platform such as a surface vessel, an autonomous underwater vehicle (AUV) or a glider. As can be observed, the received signal is subject to ambient noise, and the signal at the receiver originates from multiple different paths with different delays and amplitudes.

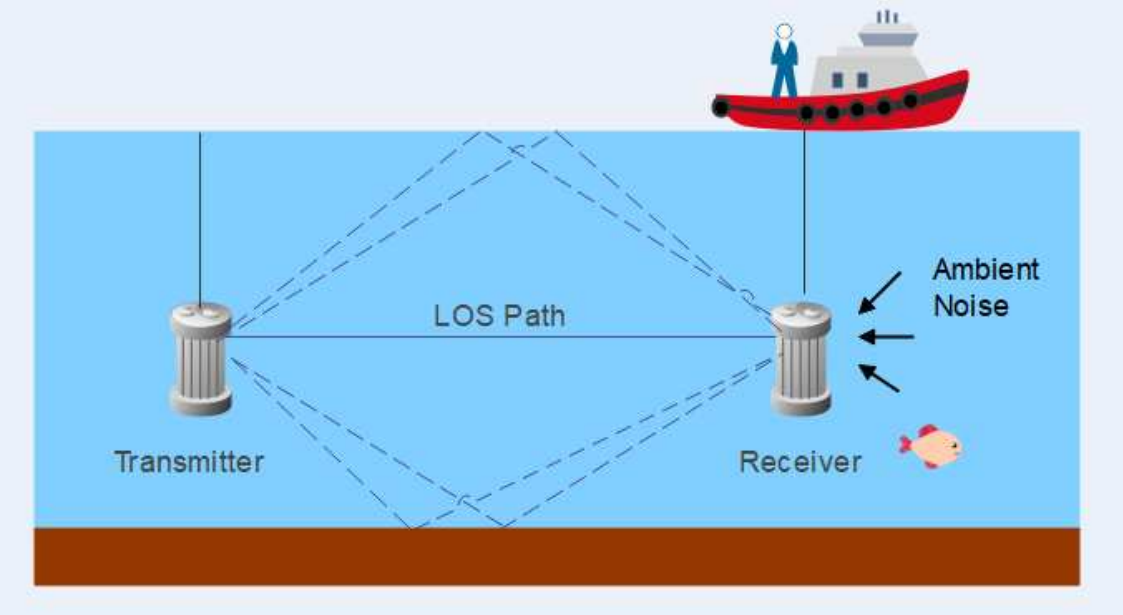

Figure 1.2: Channel impairments in an underwater channel

In practice the propagation channel has a number of impairments that deteriorate the reliability of the physical layer. Specifically, underwater acoustic propagation is characterized by high attenuation, multipath propagation, and time-varying Doppler shifts that can significantly impact the performance of communication systems [7]. These impairments, combined with a low bandwidth availability and limited number of usable frequency channels can largely impact the overall system performance and throughput.

It should be noted also that typical underwater communication systems are currently half duplex since a high power transmit signal is required and can saturate the receiver electronics. In order to mitigate the limitations imposed by half-duplex operation and optimize system performance, adaptive techniques and accurate channel estimation can contribute to

dynamically adjusting various parameters, such as modulation ratio, signal power, coding rates, and sub-carrier allocation, based on the estimated channel conditions. In doing so, the use of all available resources can be optimized and the overall communication performance can be improved.

1.2 Research Motivation

Because of the unique challenges posed by the underwater channel characteristics, efficient estimation of the impairment severity using low overhead on the data transfer is critical to improve the communication link power efficiency. Accurately acquiring and understanding the channel characteristics such as the average Signal to Noise Ratio (SNR), Delay Spread and Doppler Spread enables the system to better adapt and optimise its performance. Advanced signal processing algorithms and compensation techniques can be employed. Channel knowledge enables adaptive communication system with the ability to dynamically adapt for example at the physical layer the modulation ratio, the signal power, the coding rates and for multi-carrier modulation, the number of sub-carriers in the band as a function of the instantaneous or average SNR, delay and Doppler Spread.

A discovery message can be used to obtain channel propagation conditions. The channel estimation can serve to define different parameters in the communication stack, including at the Multiple Access Layer (MAC) to share the resources and the Network layer for routing purposes. It should be noted that the long latency in the transmission link prevents feeding back the small scale fading characteristics between the transmitter and receiver. Nonetheless, information about the large scale parameters can serve to optimize the communication link parameters.

Over the years, multiple studies have been conducted to develop efficient and accurate techniques to estimate channel conditions for adaptive underwater communication systems. In 2014, Wang et al. [8] proposed a channel estimation method based on a time-frequency domain by exploiting the sparsity of the channel impulse response in a joint domain. In 2020, Zhang et al. [9] proposed an adaptive channel discovery technique based on a cooperative approach that used multiple nodes to estimate the channel parameters and adaptively adjust the transmission parameters based on the channel state information (CSI). This technique was successful in enhancing performance in terms of bit error rate and throughput compared to traditional techniques. In [10], Wang et al. explored the use of Gaussian likelihood and

constellation aggregation techniques for improving the accuracy of channel estimation in underwater acoustic communication systems.

Although research on channel discovery for adaptive communication systems for underwater acoustic communication has advanced in recent years, there are research gaps such as robustness to harsh environmental factors, signal interference and frequency-dependent channel effects, optimizing the energy efficiency to support underwater devices that are often deployed in inaccessible and harsh underwater environments without compromising the communication performance, increasing number of nodes in large-scale underwater networks, lack of standardized communication protocols and interfaces, that still needs to be addressed.

Also, channel estimation techniques still face numerous challenges. Obtaining channel data can be a complex process owing to challenges in positioning sensors, limited access to specific locations, and adverse conditions for deployment. Regular channel sampling is necessary to avoid inaccuracies in estimation. Ambient and man-made noise continue to degrade the quality of received signals. Estimation algorithms demand sufficient training data to establish reliable channel models. Acquiring these large data sets can be time-consuming and resource-intensive, limiting the accuracy and validity of estimation techniques.

In this thesis, a technique for the estimation of the various channel impairments including the Doppler spread, delay spread, signal to noise ratio (SNR) and channel gain has been developed. This work seeks to address the challenge of channel latency in underwater acoustic communication systems that often impacts the reliability of instantaneous channel data for adaptive systems. By averaging channel conditions over a range of scenarios, from good to challenging, a comprehensive channel figure of merit is obtained that encapsulates the overall channel performance. The model is then applied to a JANUS compatible physical layer centered at 27.5 kHz. This approach also enhances the reliability and efficiency of underwater acoustic communication systems. It opens up new possibilities for achieving higher data rates and robustness in challenging underwater environments. In this thesis, the model to estimate various figure of merits that are intended to be sent to the nodes is described. These estimated figure of merits ultimately decide the communication link parameters such as the modulation techniques in an adaptive communication system, similarly to the technique described in [11].

1.3 Research Objectives

The objective of this thesis is to design and evaluate channel estimation algorithms for Doppler shift, Doppler spread, delay spread, and Signal-to-Noise Ratio (SNR) in underwater acoustic communication. The focus is on utilizing statistical averaging techniques to address the challenges posed by fast time-varying channel conditions and latency constraints in an underwater transmission environment. The designed algorithms are based on a JANUS-inspired discovery frame that is relying on Frequency Hopping Binary-FSK (FH-BFSK) modulation. The ultimate goal is to be able to use FSK as a probing mechanism for an OFDM based adaptive communication system that can operate at different specifications and can achieve different data rates. The number of subcarriers, modulation ratio and length of guard bands can be defined as a function of the estimated delay and Doppler spread of the transmission channel.

To accomplish this objective, the following key aspects will be pursued:

- Develop a Channel Estimation Algorithm: The thesis aims to design and develop algorithms for estimating key channel characteristics, including Doppler shift, Doppler spread, delay spread, and SNR in underwater acoustic communication systems. These algorithms will leverage statistical averaging techniques to mitigate the impact of fast time-varying channel conditions. The objective is to obtain accurate and reliable estimates of these channel parameters, enabling effective adaptation of communication systems.

- Utilize a JANUS-Inspired Frame: The research will leverage the JANUS-inspired frame based on Frequency Hopped Binary FSK modulation as a framework for incorporating the developed channel estimation algorithms. The objective is to create a discovery message that is robust to the underwater propagation impairments while also ensuring that the validity and reliability of the payload by employing statistical averaging across multiple estimations, thereby mitigating the impact of potential outliers or inaccuracies in individual runs and ensuring the preservation of meaningful information.

- Validate the Channel Estimation Reliability: The thesis will evaluate the performance of the designed channel estimation algorithms and the JANUS-inspired frame by implementing the same across a real-world underwater channel. The objective is to

assess the accuracy, reliability, and efficiency of the algorithms in estimating channel characteristics and acquiring essential Channel State Information (CSI) for adaptive communication systems. Performance metrics such as estimation error and ratio of orthogonality will be analyzed to validate the effectiveness of the proposed algorithms.

1.4 Organization of Thesis

This thesis is organised as follows. In Chapter 2, the research problem statement is delineated, forming the foundation for the subsequent literature review. The literature review comprehensively examines the recent advancements and established methodologies in channel estimation in the realm of underwater acoustic communication. Each technique's merits and limitations are evaluated. Subsequently, a brief synopsis of Frequency Shift Keying (FSK) and the JANUS protocol is provided, accompanied by an elucidation of their relevance to the field.

Chapter 3 presents a comprehensive account of the acoustic communication system model and its simulation set-up. The chosen simulation parameters and tools are justified. Additionally, a detailed description is provided for the design and implementation of the JANUS inspired discovery message. The chapter also offers a thorough exposition of the channel estimation algorithms for Delay Spread, Doppler Shift, Doppler Spread, and Signal to Noise Ratio (SNR), along with an in-depth analysis of their respective performance metrics. Subsequently, the strengths and weaknesses of each algorithm are assessed.

Chapter 4 delves into the implementation and validation of the channel estimation algorithms introduced in Chapter 3. It describes the experimental setup, including the equipment used, and provides an overview of the real-world data acquisition and analysis process. The findings of the experiments are presented, and the outcomes from simulations are compared.

Finally in Chapter 5, conclusions are presented.

Chapter 2

State of the Art on Adaptive Underwater Acoustic Communication Systems

In this chapter, a literature review is conducted on channel aware adaptive communication systems and consecutively on the developments in channel estimation techniques for underwater acoustic communication links. Channel impairments greatly affect the signal as it propagates through the underwater environment. In environments that offer varying physical conditions, the communication performance is hard to predict. An understanding of the existing adaptive communication systems is necessary to enable more efficient system design, modelling, bench-marking and performance evaluation. Understanding the existing estimation techniques is important in accurately characterizing the underwater channel to facilitate adaptive optimization and enable reliable communication in harsh UWA environments.

2.1 Channel Aware Adaptive Communication Systems

An adaptive communication system for underwater acoustic communication links can be crucial due to the underlying harsh channel conditions that pose significant propagation challenges due to attenuation, scattering, multipath and the complex interaction of acoustic waves with the water medium. An adaptive link is an instrumental step towards establishing a real-time, energy efficient link with optimized throughput and minimized channel impairments such as Doppler shift, delay spread, and latency. The existing underwater acoustic modems and the literature currently available in the market either propose robust but low-rate solutions in the range of a few 100 bits per second for longer distances or high-speed solutions for medium and short ranges. The first category works by using a symbol duration greater than the maximum propagation delay of the channel using a spread spectrum approach or by techniques such as frequency hopping as in the JANUS standard. The second category of solution tackles the issue of limited bandwidth and inter symbol interference by using multi carrier modulations to achieve a greater throughput. However, the challenge lies in using multi carrier modulation techniques such as OFDM due to its sensitivity towards

frequency offsets, High Peak to average power ratio (PAPR), and frequency selective fading. Any approach to deal with motion induced Doppler effect in these situations can significantly reduce the data throughput. Mangione et al. in [12] proposed a simple technique wherein they periodically estimated the channel spreading parameters instead of implementing a complete Doppler compensation technique. Based on the characterized channel, the OFDM in parameters where dynamically adjusted. The design and implementation of a software defined modem was presented in this work which was capable of estimating the channel characteristics and dynamically adjusting the parameters of the OFDM modulator as a function of the channel environment. The system had a capability to switch to a JANUS based FSC modulation when the conditions of the channel became particularly harsh. This work concludes that an optimized adaptive OFDM communication link can be established with a minimized inter symbol interference by dynamically adjusting the optimum number of subcarriers and CP length.

Demirors et al in [13] present a high-rate software defined underwater acoustic modem with real time adaptation capabilities in applications that specifically demand high data rates such as real time video transmission in underwater channels. A high-rate software defined acoustic modem capable of reconfiguring its physical layer in real time in the presence of fast varying channel conditions was presented. For this a zero-padded OFDM (ZP-OFDM) link was used to solve a rate maximization problem under predefined BER reliability constraints with achieved rates of up to 260 kbits/second. However, this throughput was achieved over only 200 meters in shallow water using a robust chirp based feedback channel.

The performance of an adaptive communication system depends on the transmitter's knowledge of the channel that is sent as feedback by the receiver. It can be a challenging task to characterize a channel and send this information back to the transmitter specially over long distances owing to the slow speed of acoustic waves. Radosevic et al. in [14] designed an adaptive OFDM system capable of estimating very small Doppler rates in mobile systems to then account for highly stable Doppler compensation over long intervals of time. The work proposes to identify and estimate only the significant paths of a channel with a large delay spread and treat the statistical properties of channel fading as unknown to adaptively compute the parameters of linear predictors using Recursive Least Square (RLS) algorithm. While an initial scheme was drawn aimed to adjust the modulation level assuming uniform power allocation over all subcarriers, a more advanced scheme was designed that aimed at

adjusting both the modulation level and the power allocation for each subcarrier.

Blom et al. in [15] presents the development of a physical layer for adaptive underwater acoustic communications that focuses on utilizing a frequency repetition spread spectrum (FRSS) physically capable of dynamic reconfiguration. These developments, also referred to as "Smart Adaptive Long and Short Range Underwater Acoustic Network" or SALSA, combinedly referred to as the FRSS-SALSA, supports the automatic configuration switching based on obtained channel and noise conditions which the most relevant descriptor for profile switching being rate independent output SNR. It uses a coded preamble that is capable of simultaneous detection, synchronisation and communication.

It is possible for a modulation scheme designed for a specific channel model to underperform when the channel characteristics undergo a change. To select signals from a broad range of bits, Pelekanakis et al. in [16] was the first to propose the use of decision trees to extract the relationship between Bit-error Rate (BER) and acoustic channel characteristics following the idea that it is impossible to find general probabilistic models for channel multipath and Doppler spread due to the complex physical properties determining sound propagation.

In recent years, the subject of adaptive underwater acoustic communication systems has seen tremendous developments, prompted by the need to address specific challenges imposed by the underwater environment. It is clear that adaptive approaches play a critical role in improving the reliability, effectiveness, and robustness of communication links beneath the water's surface. However, while these systems provide significant benefits, they are not without constraints. The high computational cost of adaptive algorithms, susceptibility to noise and interference, and the requirement for real-time channel information to cater to fast varying channel conditions are all current research and development challenges.

In this thesis, the primary objective is to develop a multi-carrier modulation system capable of dynamically adjusting its parameters to optimize or maintain a desired throughput in the underwater communication link. This entails characterizing the underwater acoustic channel and sending this data back to the transmitter for dynamic adaptation of subcarrier size or modulation ratio. The proposed Phorcys [17] paradigm builds upon the JANUS [18] protocol, aiming to deliver secure, reliable, and efficient underwater communication. Therefore, the focus is on designing efficient channel estimation techniques to enhance the feedback

link's efficiency and accuracy within the adaptive communication systems. By employing sophisticated channel estimation algorithms, the system can extract essential channel information while minimizing the data size and latency. This approach ensures that the transmitter can continuously optimize its modulation scheme and subcarrier configuration, responding dynamically to changing channel conditions and achieving improved communication performance.

2.2 Orthogonal Frequency Division Multiplexing for Long-range Mobile Communications

The recent surge in explorative and shipping activities in the Arctic has highlighted the growing need for dependable wireless communication links on mobile platforms in this region. To address this requirement, the Defence Research and Development Canada conducted a significant sea-trial [19] in the summer of 2019 near the Gascoyne Inlet, close to the Barrow Strait in the Canadian Arctic. During the experiment, the system produced underwater acoustic signals, which were transmitted and captured by a network of 9 hydrophone receivers. To evaluate the system's performance, various source-receiver separation distances were tested, ranging from 10km up to 35km. The transmissions received at the hydrophone array were meticulously recorded for later decoding and analysis upon the conclusion of the experiment.

The recorded data was used to investigate the reliability of an Orthogonal Frequency Division Multiplexing (OFDM) system [20]. The channel characteristics were extracted to establish the underlying causes affecting the system performance. A secondary objective was to define and optimize system design parameters like sub-carrier and guard band length as a function of the extracted channel Delay Spread and Doppler spread. Frequency Shift Keying (FSK) although a more common choice of modulation technique for underwater acoustic communication systems can deliver lower throughput due to its non-coherent nature. An FSK payload was also implemented to establish a reference parameter against the OFDM system in this investigation.

2.2.1 The OFDM Physical Layer

A communication system based on an M-sub-carrier Orthogonal Frequency Division Multiplexing (OFDM) scheme was proposed for a study on the performance of OFDM for long-range underwater communications under mobile conditions [20]. Instead of employing cyclic

prefixing (CP), the system adopts zero-padding (ZP) technique. The rationale behind this choice stems from two primary advantages it offers. Firstly, ZP reduces energy consumption compared to using a cyclic prefix, making the system more energy-efficient. Secondly, ZP provides greater flexibility by enabling the guard interval to exceed the orthogonality interval of the OFDM symbol. This proves valuable in scenarios where the channel exhibits long delay spread due to multipath arrivals.

At the transmitter, the $2M$-element coded data vector $\mathbf{c_M}(i)$ for OFDM symbol i is modulated using Quadrature Phase Shift Keying (QPSK) to produce $\mathbf{s_M}(i)$, followed by an M-point Inverse Fast Fourier Transform (IFFT) and zero padding, which adds $\mathrm{ZP_L}$ trailing zeros.

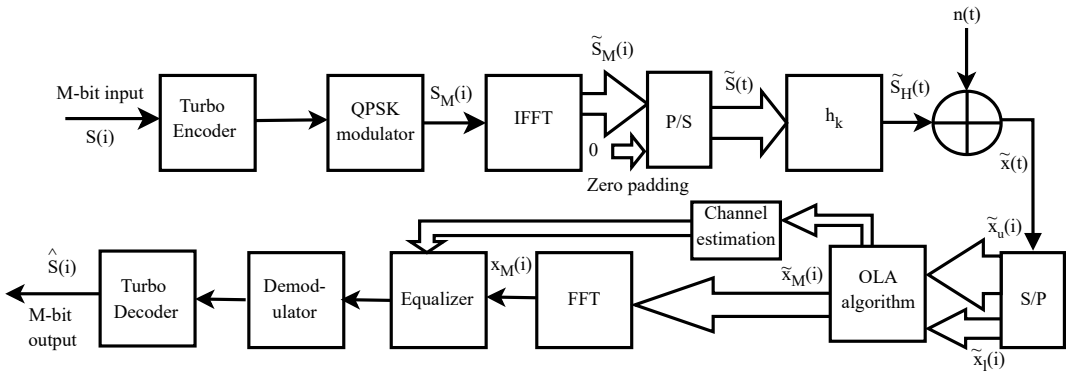

Figure 2.1: Physical layer of the modelled ZP-OFDM communication system

The time-domain blocks are serialized, filtered using a raised cosine filter with a rolloff factor of 0.25, up-converted to the carrier frequency and transmitted using a sound source. In simulation, the baseband channel is modelled by a finite impulse response (FIR) filter of order L and additive white Gaussian noise (AWGN) of variance ${\sigma_n}^2$. The FIR filter coefficients represent the complex amplitude of the channel impulse response $\mathbf{h}$. The system is designed such that $\mathrm{ZP_L} \geq L$.

At the receiver, the overlap-and-add (OLA) algorithm is implemented to recover the cyclical property of the Fast Fourier Transform (FFT) operator, as described in [21]. To estimate the channel, a Least Mean Square (LMS) algorithm is implemented due to its computational simplicity to estimate the channel. Block channel estimation is utilized to estimate the channel at regular intervals in the frame. The frequency domain signal $\mathbf{X}_M(i)$ at the output of the equalizer is QPSK demodulated to generate the $2M$-bit output for each

OFDM symbol. At the output of the QPSK demodulator, a maximum a posteriori (MAP) Turbo decoder is implemented to recover the data.

2.2.2 Measured Performance

The measured performance of the OFDM link is analyzed and compared to that of an FSK reference communication link. The measured performance is also compared to that using a model of the system. Four measured OFDM frames in different channel conditions [20] are chosen to be representative of different channel conditions. The measured channel conditions are summarized in Table 2.1, along with the measured uncoded bit error rate (BER). The table also includes a modelled BER. The model simulation is representative of the system described in 2.2.1 and using the measured CIRs extracted from the LFM.

Table 2.1: Channel reliability vs. conditions.

	SNR [dB]	τ_{RMS} [msec]	D_S [Hz]	BER (1 RX)	BER (K RX)	BER (model)
$\|h_4[k]\|$	13.5	0.9	1.33	0.07	0.02	≤ 0.001
$\|h_6[k]\|$	16.3	7.6	1.43	0.09	0.05	0.05
$\|h_{32}[k]\|$	5.5	4	1.39	0.18	0.08	0.02
$\|h_{14}[k]\|$	10.6	99	3.9	0.22	0.28	0.1

The uncoded simulated performance is shown in Fig. 2.2 as a function of SNR [20]. As can be observed, for an RMS delay spread below 5 msec ($h_4[k]$ and $h_3 2[k]$), and it is possible to converge to a BER below 10^{-3}, for an SNR below 13 dB. However, for $h_6[k]$ and $h_{14}[k]$, the CIR extends over several taps, and the performance degrades, such that at SNR = 15 dB, the BER is still above 0.03.

To evaluate the OFDM performance, synchronization to the start of the frame is performed using the refined time delay estimated at the output of the LFM cross-correlation [20]. The signal is down-converted, and for each OFDM symbol i, the phase error $\theta_{e,i}$ is estimated using the discrete Fourier transform $\mathcal{F}[\tilde{\mathbf{s}}_M(i)\tilde{\mathbf{x}}_M(i)]$, and extracting the phase at DC. Each OFDM symbol vector is multiplied by $e^{-j\theta_{e,i}}$. To equalize each OFDM symbol, a channel is estimated at regular intervals, and its estimate is used for equalization as described in Section 2.2.1. The channel estimate is obtained using a subset of the OFDM symbols. In fact, in a first instance, the performance is evaluated using 30 of the 60 symbols as pilot

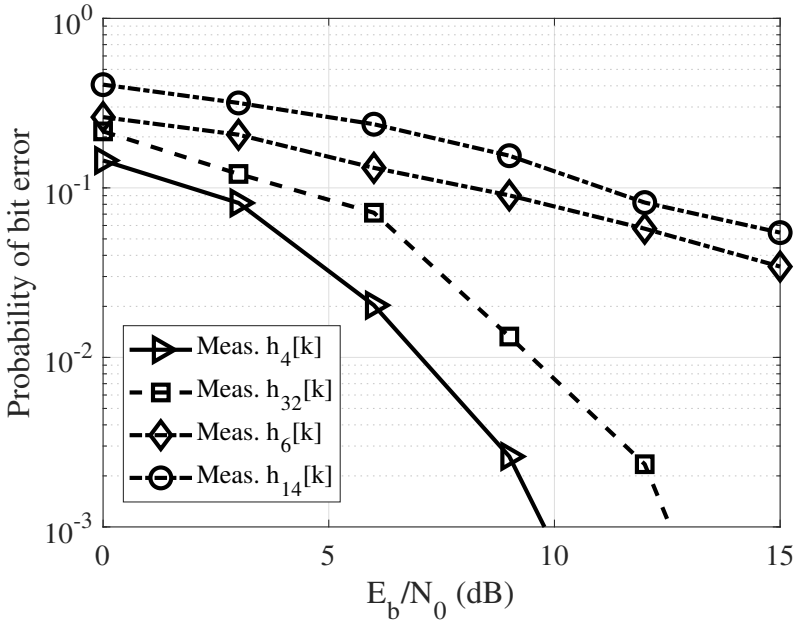

Figure 2.2: Simulated OFDM BER using measured CIRs

(dividing the overall user throughput by 2); in a second instance, the performance is evaluated using 4 pilot symbols of 60, reducing the throughput by 1/15. The performance is also evaluated at the output of a spatial combiner that simply sums the equalizer output of all hydrophones [20].

The OFDM performance is shown in Fig. 2.3 for all the transmitted frames in the measurement trial [20]. It was observed that the link is completely unreliable when the hydrophones drift lower in the water column, between measurement indices of 15 and 22. Using four pilot tones instead of 30 degrades the performance. The spatial combining was observed to reduce sensitivity to the channel impairments. The measured performance, even after spatial combining was found to be poorer than the predicted performance by simulation. This can be attributed to the Doppler spread behaviour.

2.2.3 Optimisation of OFDM parameters

In order to maximize the bitrate constrained on inter-carrier interference (ICI) and inter-symbol interference (ISI), an optimum number of sub-carriers, equal to the FFT size $N_{FFT,opt}$ can be defined. For this purpose, first, a minimum FFT size $N_{FFT,min}$ is defined that ensures that there is no ISI. To optimize the spectrum efficiency, it should be defined to be

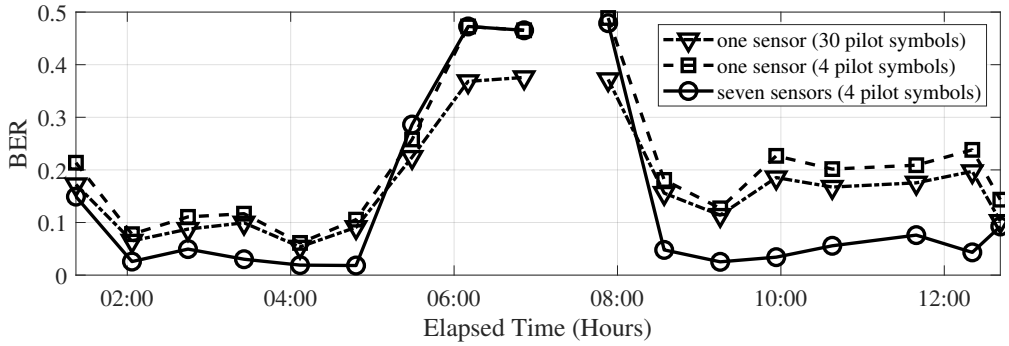

(a) Uncoded performance

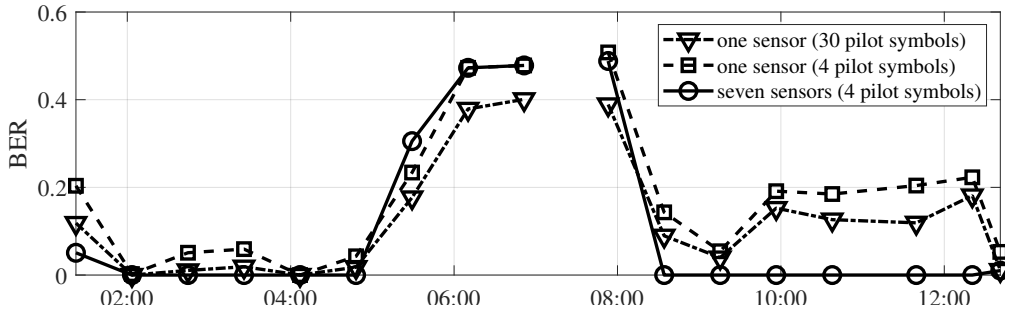

(b) Coded performance

Figure 2.3: Measured Bit Error Rate

greater than the guard interval length ZP_L, where ZP_L/R_s must always be greater than the RMS delay spread τ_{RMS}. For this exercise, we defined $N_{FFT,min} = 10ZP_L$. Similarly, the maximum FFT size $N_{FFT,max}$ is defined to be less than the channel coherence time T_C, defined as $T_C = 0.08/(D_sB)$, where D_s is the Doppler spread [22]. The optimum FFT size $N_{FFT,opt}$, for a given doubly spread channel is equal to $N_{FFT,max}$. The bitrate for these different conditions is equal to $R_b = (2R_s/3) \cdot N_{FFT,opt}/(N_{FFT,opt} + \mathrm{ZP}_L)$, where R_s is the QPSK symbol rate. Based on the optimization mapping image presented in Figure 2.4, it can be inversely stated that given the knowledge of the delay and Doppler Spread of a channel, it is possible to find the optimum number of subcarriers or the modulation ratio for a given communication link in an adaptive communication system for a specific data throughput.

2.3 Conclusion

2.3.1 Conclusion

Based on the performance analysis of the measured OFDM and FSM reference communication link it was clearly established that the performance of coded OFDM link with array

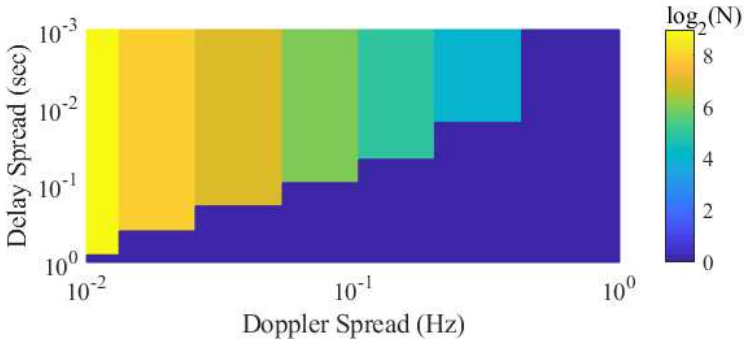

Figure 2.4: Optimum FFT Size vs. Doppler and Delay Spread

combining at the receiver is comparable to the performance of uncoded FSK, This establishes the reiterated fact that FSK fares significantly better in harsh channel conditions, thereby establishing FSK links as the choice of modulation for channel characterisation in an adaptive communication system.

2.4 Underwater Channel Estimation

In this section, a brief literature review for the state of art in channel estimation techniques for underwater acoustic communication systems is presented. The underwater acoustic communication channel has characteristics defined by multi-path due to acoustic wave reflection off of multiple surfaces before reaching the receiver, noise and interference, Doppler effect due to relative motion between transmitter and receiver, and frequency selective fading. Channel estimation allows for a better understanding of the various propagation paths and their delays, as well as the improvement of Signal to Noise Ratio (SNR) by separating the signal and noise components, proper Doppler estimation and compensation, and characterization of frequency dependent fading components. The propagation channel itself has limitations: the channel capacity depends on the distance, transmitter motion will introduce a Doppler spread, the signal bandwidth is inherently low, there is severe attenuation from the properties of the water as a function of frequency, and there is time varying multipath. In fact, as throughput requirements are increasing, the communication link quality becomes very sensitive to the channel impairments. Fundamental limitations of the acoustic channel were first presented in [23].

Channel estimation serves in adaptive communication systems to continually assess the channel's status and adjust transmission parameters in real-time for optimal performance.

Channel characterization can be used to choose the best modulation scheme, coding rate, and power level for the present channel characteristics. This optimization results in more efficient data transfer and reduced error rates. Adaptive systems can also employ channel estimate data to dynamically modify transmission power levels which guarantees that devices only transmit with the power required to maintain reliable connectivity, resulting in energy savings.

Liu et. al. in [24] proposes to use a Pseudo-Random Noise (PN) Sequence based method for channel and Doppler Estimation. The Doppler estimation method uses a delay cross correlation as opposed to Linear Frequency Modulation (LFM) based cross correlation and the channel estimation utilizes a PN Sequence based decision feedback loop. Based on the idea that the channel impulse response (CIR) of an underwater acoustic (UWA) channel is often sparse i.e. only a small number of channel coefficients are non-zero,the work in [25] proposes exploiting this sparsity of the channel to use a compressed sensing (CS) technique for channel estimation. The authors, here, model the UWA channel as a Bernoulli-Gaussian mixture random process and estimate the multipath by exploiting the channel state information under Bayesian frame first by locating the channel tap positions followed by estimating the coefficient of these taps. This technique called the Fast Bayesian Matching Pursuit (FBMP) proves to be efficient and rapid in estimating parameters of interest from collected data. As opposed to this research, Long et. al. in [26] suggests obtaining higher performance gains by exploiting the channel sparsity using a Sparse Bayesian Learning (SBL) that yields a much lower estimation error over CS in a channel environment with impulsive noise. In the research conducted by Su et al. in [27], a fast method for estimating underwater acoustic (UWA) multipath channels using Linear Frequency Modulation (LFM) signals was employed. In this approach, the sender transmits an LFM signal with pre-defined characteristics, and at the receiver's end, a correlator function is applied. This function detects significant peaks that correspond to the arrival time of the direct signal path.

In [12], a Least Square (LS) estimate obtains the CIR by using a 'sounding sequence' given by samples of the transmitted sequence and made of periodic repetitions of chirp like signals. To estimate the Doppler Spread, the channel frequency response is calculated by using the Fast-Fourier Transform (FFT) operation on the estimated CIR followed by the the auto-correlation of each frequency sample, along the channel-estimate-index dimension. The DFT of the average of these auto-correlations yield the Doppler Spectrum estimate.

In 2022 [28], Wang et al. presented reinforcement learning (RL) based UWA channel tracking using a technique called the Adaptive Subspace Tracking with Reduced Rank Model based Amplitude Estimation (ASRMAE) to follow and track the channel changes over time. An RL technique improves the channel tracking over time with the advantage of better decision making. An adaptive forgetting factor introduced into the tracking method allows for dynamic adjustment based on channel conditions over time.

The UWA channel can be represented to have a block structure which can be exploited using a block space pursuit (BSP) to derive a joint sparse recovery algorithm (DSP) [29] as is proposed in [30]. This was shown to be particularly efficient in long range UWA channel estimation. However, the proposed estimator is tailored only for sparse channels which can be characterised to have a block structure with time invariance and a long delay spread.

Another popular technique to estimate CSI especially in OFDM based communication systems is the use of Kalman filters. In [31], a Kalman-like filter is presented that optimizes the communication parameters including the length of the Cyclic Prefix (CP). The method proposed involve joint prediction and estimation at the cost of extensive simulations. Channel prediction is often considered a better approach as opposed to channel estimation owing to the fast varying nature of most channels. Channel prediction uses predictors derived from channel statistical models from algorithms such as Recursive Least Square (RLS) or deep neural networks. The suggested technique is shown to reduce overhead data that needs to be transmitted back to the transmitter in an adaptive communication link.

Doppler effect often causes additional difficulties in processing the received signal. In [32] Trubuil and Chonavel. proposed a novel algorithm to estimate the Doppler frequency by transmitting training sequences in the beginning and at the end of the transmission data frames. A cross-correlation of these training sequences yield a coarse and a precise Doppler frequency estimate with the precise estimation having a smaller ambiguity range than the coarse estimate. Conveniently, the coarse and precise estimation phases can be combined for an improved Doppler estimate. Following this work, in 2014 [33], Trubuil et al. provides another novel Doppler estimation technique for OFDM based modulation system with two training sequences at the beginning of the OFDM data frame. The findings reveal that the training sequences' power spectral density covers the channel frequency response with negligible fading, making them ideal for an additional effective channel estimation over the frequency range.

In [34], the study proposes an improved Doppler estimation technique centred around a virtual time reversal mirror that dynamically matches multipath time-varying channels by concentrating the synchronous head of two neighbouring fame-signals in the time domain, properly measuring the frame length, and estimating the Doppler shift. It enables any communication system that transmits signals frame by frame to use the technique without additional aiding signals at the price of an increase in processing cost.

Underwater environments present distinct challenges, emphasising the importance of precise and resilient channel estimate algorithms. According to the research reviewed, channel estimation is critical not only for reducing the adverse effects of these issues, but also for allowing adaptive communication techniques that optimise data rates, power allocation, and error correction. The strategies presented, which range from Bayesian statistical approaches to adaptive algorithms, demonstrate the many ways utilised to solve channel estimates in underwater environments. As technology advances, the use of machine learning and reinforcement learning techniques increases the possibility of enhanced channel tracking and prediction. Further study in this area holds the potential of more robust, efficient, and dependable underwater communication systems, which will contribute to breakthroughs in domains as diverse as marine exploration, environmental monitoring, and autonomous underwater vehicles.

2.5 Relevance of FSK in UWA Communication

Frequency-shift keying (FSK) is a way of transferring discrete digital signals using the two binary states – logic 0 (low) and 1 (high) - are each represented by an analog waveform. Logic 0 is represented by a certain frequency, while logic 1 is represented by a different frequency. The deviation or shift point is the distance between logic 0 and logic 1. When transmitting data between nodes, the distance between these digital states determine how much data can be delivered in a specific period of time. If the logic 0 and logic 1 states are too widely apart, the throughput will be low. If the frequency shifts are too close together, however, it might induce inter-symbol interference (ISI) in the data frame. Frequency-shift keying has been around for a while. It was developed in the mid-1900s for use in mechanical teleprinters. The standard speed of these devices was 45 baud. FSK also stands to be one of the earliest form of modulation in acoustic modems for underwater communication. FSK employs an energy-detection or a non-coherent algorithm rather than the phase-detection (coherent)

algorithm that intrinsically makes it robust to the time and frequency spreading of the channel. In the context of underwater acoustic communication, FSK has the inherent benefit of frequency diversity, which means that the information is spread across multiple frequencies. This helps to mitigate the impacts of multipath propagation, which occurs when signals travel several pathways due to reflections and refractions in the underwater environment. An additional benefit of FSK modulation is its compatibility with adaptive modulation approaches, allowing adjustments in the modulation index or the quantity of frequency shifts according to the prevailing channel conditions. This capability aids in enhancing performance in response to changing environmental factors.

Frequency-Hopping Frequency Shift Keying (FH-FSK) combines the advantages of FSK modulation with frequency hopping spread spectrum (FHSS) methods. The underwater environment is characterized by a relatively limited bandwidth and the possibility of intentional jamming. This necessitates the use of spread spectrum communication systems. The essential premise of spread spectrum is to distribute the energy of the signal across a wide bandwidth, therefore reducing the impact of narrow-band interference and the obstacles provided by multipath propagation.

Frequency hopping, a specific application of spread spectrum, becomes critical in such contexts. It entails rapidly switching carrier frequencies in accordance to a specified hopping pattern. This seemingly dynamic behaviour serves an important function of improving resistance to interference and jamming efforts making it extremely difficult to detect and interrupt communication owing to the quick and unpredictable frequency fluctuations. As a result, the dependability of underwater communication networks is enhanced considerably. The adaptability inherent in frequency hopping addresses Doppler shifts induced by relative device motion or dynamic water conditions, ensuring sustained communication performance. In a setting rife with ambient noise from marine life and natural occurrences, the capacity of frequency hopping to avoid frequency bands with high noise levels becomes crucial. FHSS augments communication reliability in the face of significant noise issues by intelligently selecting frequency bands with the lowest possible level of interference.

The benefits of Frequency-Hopping Binary Frequency Shift Keying (FH-BFSK) have been, hence, identified and standardised within the JANUS protocol, highlighting its importance in UWA communication.

2.6 The JANUS standard

JANUS [18] standard was developed as a simple multi-access acoustic protocol that was designed and tested by the in NATO Centre For Maritime Research and Experimentation (CMRE) and later adopted as a NATO standard for military, civil and international adoption [35]. The JANUS standard uses a physical layer coding called Frequency Hopped (FH) Binary Frequency Shift Keying (BFSK) due to it's simplicity and robustness to harsh aquatic environments. It maps the binary data into 13 evenly spaced tonal pairs of unspecified phase across a bandwidth $B_w = \frac{1}{F_c}$, where F_c is the carrier frequency of the signal. The JANUS packet begins with a fixed preamble of 32 chirps, or 32 frequency-hopped symbols, the value of which is a pseudo-random m-sequence, followed by a "baseline JANUS Packet" encapsulating 64 bits of data. A "Cargo" packet of any length can be inserted at the end as an option. A 1/2 rate convolutional encoder provides robustness to temporal and frequency fading. The order for these 13 pseudo-orthogonal tonal pairs are chosen to provide optimal inter-symbol interference (ISI) from multipath or inter-packet collision. The sequence of the tones are considered known to all potential receivers. The standard defines a typical chip duration of 6.25 ms, resulting in an 80 bps data rate. There was a lack of standardisation in underwater communication protocols prior to the introduction of the JANUS protocol. The JANUS protocol provides a standardized framework that ensures interoperability between different systems, allowing diverse devices to communicate seamlessly, regardless of their manufacturer or intended application.

Following [35] where JANUS fast modes haven been suggested as a potential standard evolution, Li et al. in [36] used JANUS header and cargo packets for a frequency range of 100kHz to 130kHz, with a bandwidth of 30 kHz and a centre frequency of 115 kHz, keeping other parameters unchanged. This raised the bit rate of the JANUS protocol from 80 bps to 737 bps with a symbol rate of 23 ksps using either BPSK or QPSK for cargo packets. However, the results suggested that the detection and synchronization of the signal became more challenging as the center frequency was shifted upwards. The authors proceeded to suggest using JANUS not only for symbol detection and synchronization but also as the pilot to estimate the channel to determine the guard intervals needed for a given channel and improve the packet efficiency.

In [37], Baldone et. al. suggest applying a simpler Cross-Ambiguity Function (CAF) approach that may be employed in real-time applications to a JANUS preamble, which is

made up of an m-sequence of 32 pseudo-random symbols, to estimate and adjust for the Doppler effect without modifying the JANUS standard. The authors use the standard for Doppler estimation using a bank of correlators at the receiver wherein the received signal is correlated with the known waveforms (the 32-chips of the JANUS preamble), prescaled by different Doppler scaling factors.

Another step in the evolution of JANUS standard was the proposal of the Phorcys [17] paradigm. Phorcys aims to address the inherent security limitations of the JANUS protocol's built-in features by advancing the concept through the development of a secure-by-design acoustic communication protocol suite. Phorcys also seeks to tackle challenges related to the enhancement of robustness in harsh channel conditions, enabling higher data-rate modes, accommodating multiple access scenarios, and reducing the impact of interference.

Despite the recent progress made in JANUS and the introduction of the Phorcys concept, there are still research gaps in appropriately selecting the data content for transmission to the transmitter. This is due to the impracticality of transmitting extensive or complete instantaneous channel data sets, given the considerable channel latency. This thesis seeks to tackle this challenge of conveying substantial instantaneous channel data back to the transmitter by employing an averaging methodology for large statistical data-set describing the channel behaviour over a period of time.

Chapter 3

System Modelling and Methodology

Underwater acoustic (UWA) communication is grappled with multipath, attenuation, Additive White Gaussian noise (AWGN), Doppler and other impairments that can make the transmission of reliable data challenging. Innovative solutions are required to solve all of these challenges, and one such approach involves the use of probing sequences for channel characterisation and consequent parameter optimisation. This thesis proposes to exploit the relevance of probing sequences to help characterise the channel and then optimise communication system parameters, ultimately improving reliability and performance for a given throughput.

In the quest to optimise the performance of a multi-carrier modulation system, characterising the delay and Doppler spread of the channel can be pivotal, especially in an underwater acoustic link. Delay Spread is a fundamental parameter that characterizes the temporal scattering of a signal due to multipath propagation. Signals reaching the receiver undergo distinct time delays due to traversing diverse paths within the underwater setting. This temporal scattering can lead to intersymbol interference (ISI), where symbols designated for transmission in a specific time segment interfere with signals intended for communication in successive time segments. The precise assessment of delay spread enables the communication system to reconfigure its transmission attributes, such as guard intervals, modulation schemes, and transmission parameters, to minimise the effects of ISI.

Doppler spread is caused by the relative movement of the transmitter and receiver. The Doppler shift, which is caused by motion, can cause frequency dispersion in the received signal. The Doppler spread can vary dramatically in the undersea environment, where boats, underwater vehicles, and even marine life can cause motion. Effective Doppler spread estimate assists in the design of modulation schemes and signal processing systems that can handle these frequency changes. If Doppler spread is not taken into consideration, it can lead to signal deterioration, symbol misinterpretation, and overall performance decline.

The use of delay and Doppler spread estimations, in conjunction with dynamic parameter optimisation methodologies, drives underwater communication systems towards increased reliability and efficiency. The insights provided by the probing sequence analysis open up the path for parameter optimisation, which is essential in the design of adaptive underwater communication systems. The communication system responds to changing channel circumstances by dynamic parameter change, guaranteeing reliable and efficient data delivery. Modifying the modulation ratio, subcarrier switching, and altering guard interval duration are among the proposed parameter switching schemes. The modulation ratio, for example, might be tuned to achieve a balance between spectral efficiency and resilience, while subcarrier switching allows the system to make optimal use of the available frequency bands. Furthermore, changing the duration of the guard intervals accommodates various delay spreads, reducing ISI.

This proposed system aims to integrate the JANUS protocol as a transformative approach to enhance its interoperability and compatibility with other JANUS-compliant systems. This integration involves the strategic deployment of a discovery sequence designed to mimic a standard JANUS frame, primarily for comprehensive channel characterization thereby enhancing the system's performance and adaptability.

In this chapter, a detailed description of the Frequency Hopped-Binary Frequency Shift Keying (FH-BFSK) modulation based probing sequence is described. This probing sequence is implemented to act as a discover message that records and characterizes the transmission channel. In section 3.1, the modelled physical layer is described for transmission of a probing sequence. In the consecutive sections 3.3 and 3.4, the estimation algorithms for Delay Spread and Doppler Spread are given. In section 3.5, a statistical analysis of the estimated data with their respective performance metrics are provided.

3.1 A Physical Layer Model

In this section, a physical layer model that adopts several of its features from the JANUS standard is described. The JANUS standard was chosen because of its versatility, reliability, robustness to harsh channel conditions, and reduced susceptibility to interference from other sources [18]. Furthermore, the JANUS standard provides interoperability between different underwater communication systems, allowing for easier collaboration and communication between different organizations and equipment.

As shown in Figure 3.1, the physical layer described in this work is implemented based on a Binary-Frequency Shift Keying (B-FSK) technique that involves switching between two different frequencies to represent digital transformation. BFSK is a modulation scheme renowned for its effectiveness in digital data transmission. The B-FSK performs a dynamic alternation between two distinct carrier frequencies of -96 Hz and 96 Hz to convey the underlying digital information for bit "0" and "1" respectively.

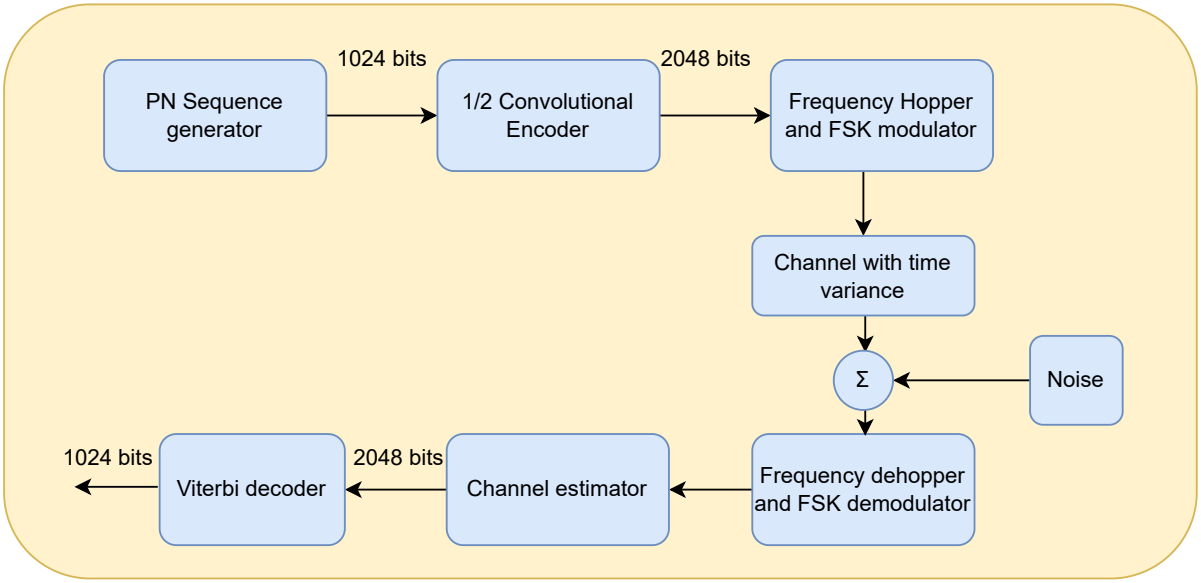

Figure 3.1: Modelled physical layer of the FH-BFSK system

A pseudo-random noise(PN) sequence with a length of 1024 bits is used as the initial data frame that serves as the discovery message for the model. This PN sequence serves as a crucial precursor to channel exploration and information exchange. The PN sequence is then encoded by a 1/2 rate convolutional encoder and then B-FSK modulated. This encoding process introduces redundancy to the sequence, enhancing its resilience against potential transmission errors. The modulated bits are subsequently subjected to a sophisticated frequency hopping strategy inspired by the work in [18]. The implemented hopping technique leverages a meticulously designed set of 13 pseudo-orthogonal tonal pairs, each pair representing two distinct frequencies that are distributed across a bandwidth of 5 kHz. The choice of tonal pairs and their even spacing serves a dual purpose: to optimally cover the available bandwidth and to ensure uniform utilization of the frequency spectrum. To maintain signal continuity and mitigate potential disruptions during frequency transitions,

the frequency-hopped B-FSK (FH-BFSK) is implemented with a continuous phase modulation (CP-FHBFSK). The use of evenly-spaced tonal pairs ensures that the hopping sequence covers the entire frequency band, thereby securing communication from interference of any kind.

A focal point of the system modelling is to assess the performance of the system under the influence of diverse and challenging conditions. To achieve this, the modelled channel is characterized by two primary factors: additive white Gaussian noise (AWGN) and an exponentially decaying channel gain. These elements closely emulate the realistic distortions inherent in underwater acoustic communication channels, wherein signals are subjected to noise and signal attenuation due to distance. Figure 3.1 is a flow diagram representation of the modelled communication link in which the FH-BFSK modulated discovery message is transmitted across a channel with additive white Gaussian noise (AWGN) and an exponentially decaying channel gain. For certain runs of the simulation, Doppler shift and Doppler spread are introduced to mimic the signal spreading and frequency shifts incurred due to the relative motion in the presence of multipath between the transmitter and receiver.

At the receiver end, the signal integrity is assessed. The received discovery sequence is frequency de-hopped, BFSK demodulated and analyzed to estimate the channel conditions. This analysis involves measuring the effects of channel gain, multipath, Doppler shift, and Doppler spread on the signal. A Viterbi decoder is then used to reconstruct the 1024 bits of the PN sequence from this de-hopped and demodulated signal. The bit-error rate for the transmission is calculated by a bit-wise comparison of the transmitted and received PN-sequence as a quantifiable measure of communication discrepancy.

3.2 The Discovery Message

In this section, a description of the modelling of the JANUS-inspired discovery frame is presented. A 1024 bit PN-Sequence constitutes the initial version of the discovery message. The PN-Sequence used is a Gold Code or Gold Sequence which is a binary pseudo-random sequence characterized by their balanced auto-correlation and cross-correlation properties, which make them suitable for spread spectrum communication systems for tasks like channel synchronization and signal multiplexing.

3.2.1 Convolutional Encoding

A rate 1/2 convolutional encoder is implemented to obtain 2048 bits aimed at enhancing the redundancy of the data frame at the transmitter. A Viterbi Decoder is used at the receiver for decoding the received demodulated signal. Convolutional coding, a type of Forward Error Correction (FEC) coding is one of the most widely used error correcting codes. Unlike in block codes where the data stream is divided into blocks of bits with a specific length, encoded by parity bits, in convolutional codes only the parity bits with possible errors are received by the receiver. Convolutional encoding with Viterbi decoding is particularly suited to a channel in which the transmitted signal is corrupted mainly by additive white Gaussian noise (AWGN). The constraint length in a convolutional encoder corresponds to its overall window size in bits. Code rate is the ratio of the number of output bits to the number of input bits. It signifies the level of redundancy added to the original data during the encoding process. The choice of code rate in convolutional encoding affects the trade-off between error correction capability and data efficiency. The convolutional encoder used in the simulation uses a constraint length of 9 and a code rate given by 1/2. The generator polynomials used by the convolutional encoder can be represented as a function as follows:

$$g1(x) = x^8 + x^7 + x^5 + x^3 + x^2 + x^1 + x \tag{3.1}$$

$$g1(x) = x^8 + x^4 + x^3 + x^2 + x \tag{3.2}$$

A comparative study on the performance of a BFSK system with and without encoding was conducted for various constraint length, k. The bit error rate performances for coded and uncoded systems are presented in the figures 3.2a and 3.2b for hard decision and soft decision Viterbi decoding respectively. The outcomes underscore the necessity of employing convolutional encoding as a means to uphold the integrity of the data.

3.2.2 Frame Parameters

The 2048 encoded data bits are subjected to frequency hopping across 13 pseudo-orthogonal pairs of tones or 26 subcarriers, following the sequence: 7, 12, 8, 6, 9, 1, 4, 3, 5, 10, 11, 2, and 13. This is succeeded by Binary Frequency Shift Keying (BFSK) modulation with -96 Hz for digital logic "0" and 96 Hz for logic "1", contained within a 5 kHz bandwidth. The FH-BFSK signal then transitions to continuous phase modulation for signal continuity.

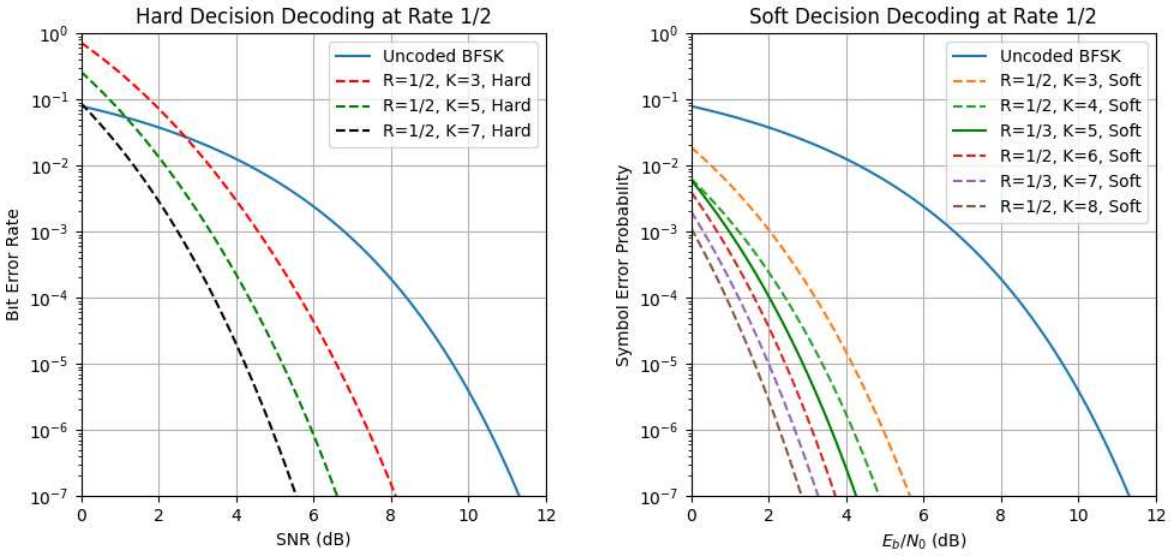

(a) BER vs. SNR for hard decision decoded BFSK

(b) BER vs. SNR for soft decision decoded BFSK

Figure 3.2: Bit error rate performance of coded BFSK vs. uncoded BFSK

This signal is later upconverted to a 27.5 kHz pass-band frequency for seamless compatibility with transmission equipment.

Table 3.1: Parameter specifications for the discovery message

Parameter	Value
Carrier Frequency	-96 Hz, 96 Hz
Passband Frequency	27.5 kHz
Bandwidth	5 kHz
Clock Frequency	24 kHz
Oversampling rate	480
Symbol period	20 msec
Frame duration	40.9 sec

Table 3.1 summarises the various parameters used to define the JANUS-like probing sequence. The symbol period of 20 msec was chosen to account for the large delay spread that can be expected in shallow water conditions. The bit rate is equal to the symbol rate of 20 ms, where each encoded bit is considered as a complete symbol. Figure 3.3 provides a spectrogram representation of a single FH-BFSK modulated frame that is intended to be used as a discovery message in an adaptive UWA communication system.

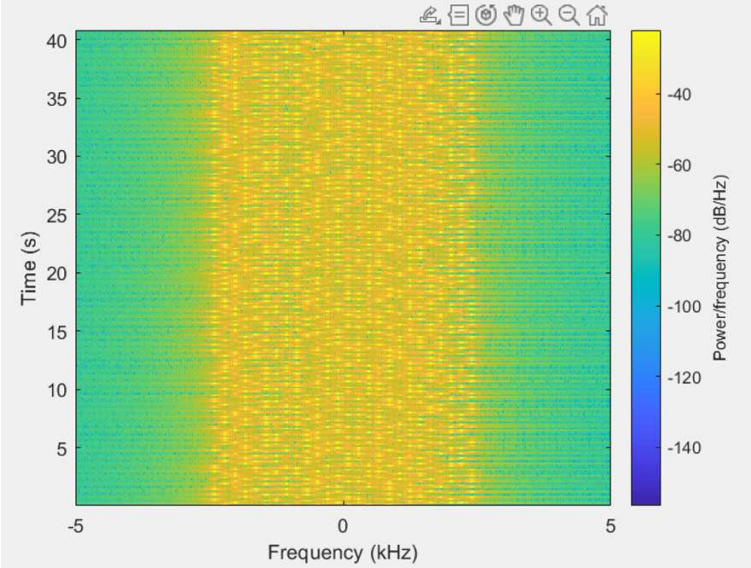

Figure 3.3: Spectrogram of a single FH-BFSK modulated frame

3.3 Estimation of Delay Spread

This section centers on the simulation of multipath propagation within an underwater acoustic channel, as well as the corresponding estimation of the channel frequency response and characterization of the channel delay spread at the receiver in the subsequent subsections.

3.3.1 Modelling of multipath in channel

In the process of simulating an underwater acoustic communication model, one of the primary intentions was to model the transmission medium to evaluate the robustness of the transmitted signal and reliability of the estimation algorithms. Within the scope of this section, the modelling of various impairments within an underwater acoustic medium has been detailed.

In any wireless communication system, the channel impulse responses can be represented as a series of pulses due to the effects of multipath propagation. The delay profile is a representation of the delays or time intervals for these various path arrivals. The maximum delay time spread of the channel denotes the entire time window that constitutes the arrival of reflections bearing substantial energy. The root-mean-square (RMS) delay spread τ_{RMS} is the standard deviation of the delay of reflections, accounting for the weighted distribution of the delays, where the weights correspond to the energy contained within the reflected

waves. To replicate the delay profile of a channel with prominent multipath, an exponentially decaying path gain model was adopted. A thorough examination of channel configurations was conducted, encompassing a wide array of decay rates. This comprehensive investigation aimed at replicating a broad spectrum of channel scenarios, extending from instances with minimal multipath effects to those closely resembling the pronounced multipath conditions encountered in real-world situations. The initial simulation was conducted with a modest decay rate of approximately 10 and subsequently automated to extend a single simulation to cover an expansive range of decay rates, increasing logarithmically. A total of 262144 delay intervals were employed. The aim of this extensive variation was to achieve a Root Mean Square (RMS) delay spread higher than 10ms.

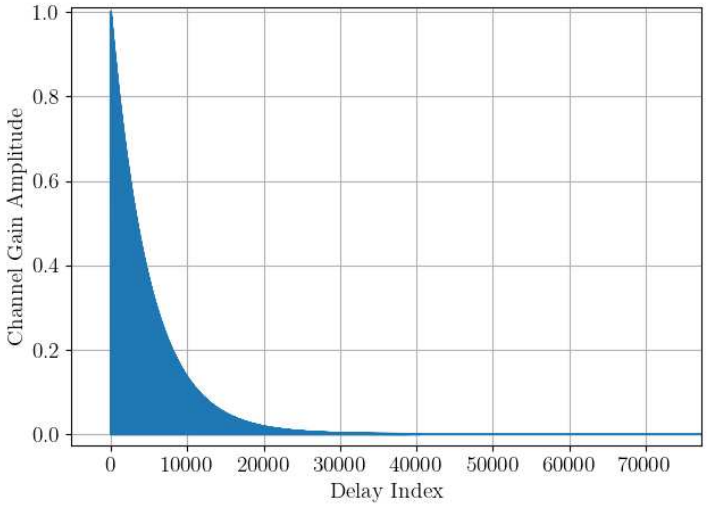

Figure 3.4: Impulse response of the modelled multipath channel

The range for decay rates that were used in the modelling are defined as

$$\alpha = [10^0, 10^{0.2}, 10^{0.4}, ...10^{4.8}] \tag{3.3}$$

This establishes an exponentially decaying multipath channel that spans RMS delay spread of 0 through 100 ms.

For each decay rate, $\alpha[k]$, in the list, the delays were arranged as

$$\tau = [0, 1, 2, ..., 262143] \tag{3.4}$$

τ represents the number of delay samples present in each multipath channel irrespective of the decay rate α.

For each delay index i, $\tau[i]$, the equation for the channel impulse response, h_k, is presented in equation 3.5.

$$h_k[i * 5] = e^{-\frac{\tau[i]}{\alpha[k]}} \tag{3.5}$$

Each impulse was periodically placed at every 5th sample in the multipath channel to establish a structured representation of the channel. Periodically spaced impulses enable the capturing of the delay spreading characteristics of multipath propagation. The impulse response of the modelled multipath channel with the highest maximum delay spread is presented in figure 3.4. The simulation effectively captured the various degrees of temporal dispersion of signals caused by multipath propagation in an UWA communication scenarios.

Considering that the modelled multipath has a total of L paths, and the gain of the ith path is given as g_i, the fraction of power in each path, b_i can be given as

$$b_i = \frac{g_i}{\sum_{j=0}^{L-1} g_j}. \tag{3.6}$$

Given that the delay if the ith path is given as τ_i, the average delay, $\hat{\tau_i}$, can be expressed as

$$\hat{\tau} = \sum_{i=0}^{L-1} b_i \tau_i = \sum_{i=0}^{L-1} \frac{g_i \tau_i}{\sum_{j=0}^{L-1} g_j}. \tag{3.7}$$

The mean squared delay, τ_{MS}, is given as,

$$\tau_{MS} = \sum_{i=0}^{L-1} b_i (\tau_i - \hat{\tau})^2. \tag{3.8}$$

Consequently, the Root Mean Squared delay spread of channel can be mathematically expressed as,

$$\tau_{RMS} = \sqrt{\sum_{i=0}^{L-1} b_i (\tau_i - \hat{\tau})^2} \tag{3.9}$$

which can otherwise be expressed as

$$\tau_{RMS} = \sqrt{\sum_{i=0}^{L-1} \frac{g_i (\tau_i - \hat{\tau})^2}{\sum_{j=0}^{L-1} g_j}} \tag{3.10}$$

The multipath modelled in this work features an exponentially decaying path gain, α given by, h_i, which denotes the channel impulse response at ith path for time delay tau.

$$h_i = \exp(-\tau/\alpha) \tag{3.11}$$

Replacing the power component in equation 3.10 with ${h_i}^2$, the RMS delay spread can be expressed as,

$$\tau_{RMS} = \sqrt{\sum_{i=0}^{L-1} {h_i}^2 (\tau_i - \hat{\tau})^2} = \sqrt{\sum_{i=0}^{L-1} e^{(-2\tau/\alpha)} (\tau_i - \hat{\tau})^2} \tag{3.12}$$

From this relationship established between the channel impulse response, channel gain and the RMS delay spread, it can be inferred from the mathematical expression that as time delay for a specific multipath component increases, the magnitude of channel gain decreases due to the exponential decay term. The integration in the RMS Delay Spread formula accounts for the contribution of each multipath component to τ_{RMS}. Thereby, multipath components with larger channel gain values will have a more significant impact on the RMS delay spreads.

3.3.2 Characterisation of Channel Delay Spread

In this section, the algorithm used to estimate the channel frequency response at the receiver is introduced. The estimated values of frequency response of the channel are subsequently used to calculate the average and RMS delay spread of the channel.

The received signal, before the estimation of channel frequency response is subjected to frequency de-hopping and demodulation to extract the baseband signal. First, the received frame is synchronized to the start of the burst and the clock drift is compensated. The received signal $y(t)$ is then down-converted using $e^{j2\pi f_c t}$ where f_c is the bandpass frequency at 27.5 kHz.

$$y_{down}(t) = y(t) e^{j2\pi f_c t} \tag{3.13}$$

The residual time-dependent tone for the ith symbol in the received down-converted frame is equal to:

$$f_i = f_i^h + f_i^m \tag{3.14}$$

where f_i^h is the hopping frequency for the ith symbol and f_i^m is the BFSK modulation frequency for the ith symbol or the frequency offset. To estimate the channel frequency, f_i, at every ith symbol, first, the frequency offset is calculated from the hopping pattern followed by multiplying the signal to a complex exponential containing the frequency offset, $e^{-j2\pi f_i t}$. This essentially creates a hopping carrier and multiplies it with the received signal

to align the hopping frequencies.

$$y_{despread}[i] = y_{down}[i]e^{-j2\pi f_i t} \tag{3.15}$$

By further multiplying the despread signal with complex exponential containing the carrier frequency values of f_0 (-96 Hz) and f_1 (96 Hz), hypothesized modulated signals h_0 and h_1 are obtained.

$$h_0[i] = y_{despread}[i]e^{-j2\pi f_0 t} \tag{3.16}$$

$$h_1[i] = y_{despread}[i]e^{-j2\pi f_1 t} \tag{3.17}$$

The hypothesized modulated signals are integrated over the oversampled segments to enhance the accuracy of the estimation. Noise is the channel has a typical random and uncorrelated behaviour across samples, but it gets averaged out when signals are integrated over large number of samples. This results in a stronger signal compared to the noise level, improving the reliability of the estimated values.

$$h_{int0}[i] = \frac{1}{ovs} \sum_{idx*ovs}^{idx+1*ovs-1} h_0[i] \tag{3.18}$$

$$h_{int1}[i] = \frac{1}{ovs} \sum_{idx*ovs}^{idx+1*ovs-1} h_1[i] \tag{3.19}$$

where ovs is the oversampling rate and idx is the frequency offset obtained from the hopping pattern.

A matched filter algorithm is implemented over the integrated hypothesized signals to produce a vector of frequency dependent channel estimates $\hat{\mathbf{H}}_{\mathbf{est}}$, defined as $[f_0, f_1 \cdots f_{M-1}]$ where M is the number of symbols in the frame. A magnitude comparison between h_{int0} and h_{int1} decides the estimated values of the channel frequency responses for 26 subcarriers. Based on which hypothetical has the greater energy concentration, the matched filter decides whether the transmitted symbol was a 1 or a 0.

3.3.3 Statistical Analysis of Channel Data

To assess the channel estimation algorithm, a simulation of the physical layer is run. The transmitted signal is applied to an exponentially decaying multipath channel with unit energy.

$$h(\tau) = \exp(-\tau/\alpha) \tag{3.20}$$

The simulation is run for multiple iterations, each time increasing the exponentially decaying factor α; for each run, the root mean square (RMS) delay spread is recorded for further analysis. After each transmission run, the channel frequency response (CFR) $\hat{\mathbf{H}}_{\mathbf{est}}(\mathbf{f})$ vector is re-organized to group estimates that belong to the same subcarrier. For example, Figure 3.5a illustrates the estimated CFR values for a channel with an exponential decay rate of 3. Figure 3.5 represents the averaged frequency response $\overline{H_{est}}(f)$ for each subcarrier. As can be observed it is an accurate representation of the actual CFR.

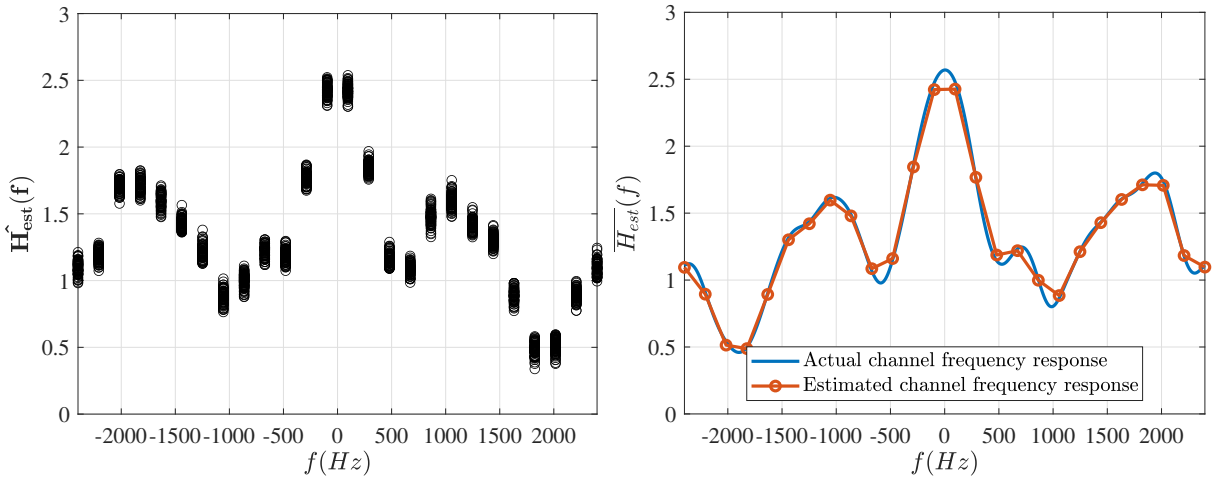

(a) Frequency dependent channel estimates vs. their respective frequencies

(b) Estimated CFR overlaid with the actual CFR.

Figure 3.5: Example of an estimated CFR.

To measure the severity of the multipath channel, the statistics of the measured frequency response $\hat{\mathbf{H}}_{\mathbf{est}}(\mathbf{f})$ are calculated. Specifically, the variance in the estimated frequency response for each subcarrier $\sigma^2_{H(f)}$ is calculated. The mean of $\sigma^2_{H(f)}$ μ_{H_f}, and variance of $\sigma^2_{H(f)}$, $\sigma^2_{H_f}$ are calculated across to obtain a single value for a given transmission, and the results are recorded. In simulation, this process is repeated for 14 different decay rates. Given that the model incorporates a random phase in the transmitted signals, the algorithm is executed 100 times to generate an averaged value for the mean, $\overline{\sigma^2_H}$, and variance, $\sigma^2_{\sigma^2_H}$, of the 26 subcarriers across the 14 different channel conditions. To maintain conformity, the RMS delay spread values for each of these channels were simultaneously recorded and averaged over the 100 simulations.

Figure 3.6 shows the plot for the mean of the variance $\overline{\sigma^2_H}$ and the standard deviation

$\sigma_{\sigma_H^2}$ of the variance for the channel estimate plotted against the RMS delay spread. Initially, this plot was constructed for smaller RMS delay spreads, approximately around 3 ms. Subsequently, an experiment was undertaken at the Aquatron Pool facility at Dalhousie University to test for the transmission of the modeled discovery message, followed by an in-depth analysis of its performance. Upon processing and analysing the received signal from this experiment, the measured variance and mean were then recorded. However, these recorded values significantly surpassed the range of the initially considered smaller RMS delay spreads. n response, another round of simulation was conducted, wherein a channel characterized by an enhanced multipath effect was generated. This aimed to achieve an RMS delay spread of 100 ms, thus enabling the superimposition of real-world measured statistical data for extrapolation purposes. Upon overlaying the recorded channel mean and variance values onto this simulated channel statistics, as depicted in Figure 3.7, the resultant values obtained are representative of an RMS delay spread between 3.3 msec and 4.3 msec.

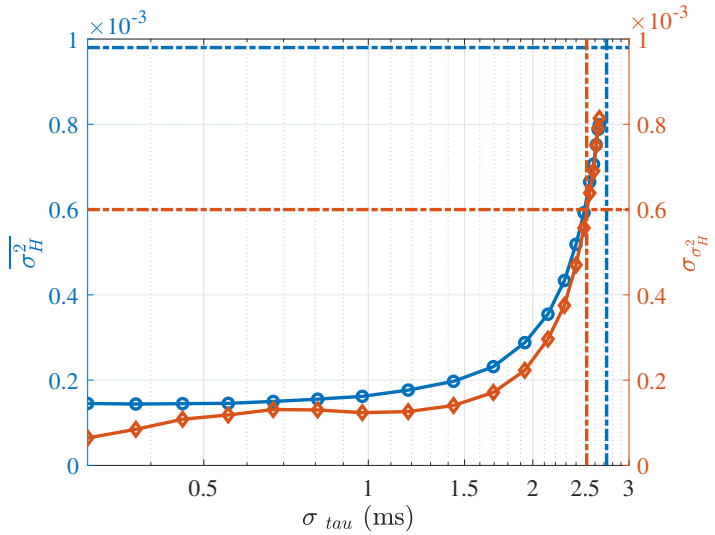

Figure 3.6: Channel mean and standard deviation for smaller RMS delay spreads

The mean and variance of an UW wireless channel can prove to be a treasure-trove of information about its expected behavior. By analyzing the mean and variance values across different channel conditions, a better understanding of the impact of different channel scenarios on the wireless channel, as well as on the channel estimation algorithm itself, can be obtained. At lower values of RMS delay spread (up to around 10 ms), the coherence bandwidth, B_c, of the channel is relatively high with the channel's frequency response remaining relatively constant across the subcarriers. This results in lower variability in the frequency

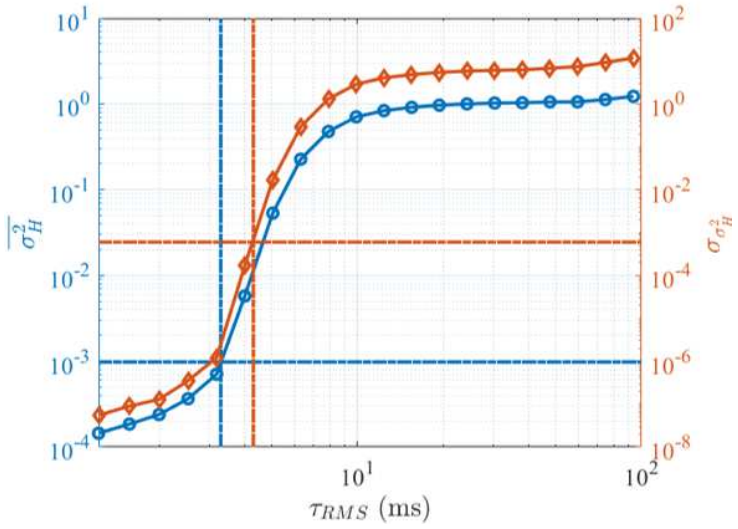

Figure 3.7: Channel mean and standard deviation against RMS delay spread of 100ms

response estimates. Therefore, both the mean and variance of the variance of the estimates remain comparatively low within this range.

As the RMS delay spread starts exceeding the coherence bandwidth (beyond 10 ms), the channel's behavior across the subcarriers begins to vary more significantly due to multipath propagation and other time-dispersive effects. This results in higher variability in the frequency response estimates across the 26 subcarriers. An increase in the mean of variance indicates that the channel is experiencing higher levels of multipath, scattering, or other factors contributing to fluctuations. Similarly, increasing variance of variance indicates a lessening of consistency in channel characteristics.

Once the RMS delay spread surpasses B_c, the channel's characteristics exhibit a relatively stable pattern across the subcarriers. This leads to a possible slowing of the variability of the frequency response estimates. The statistical values in a linear context are still growing, but at a diminishing pace. The channel's responses become less influenced by rapid changes in multipath components, and the frequency response estimates become more stable simplifying the channel estimation process. This is indicative of an optimal range of RMS delay spreads where the frequency response estimation variability is controlled. Beyond this range, the variability could potentially become less influential.

3.3.4 Performance Metrics for the Delay Spread Characterisation

This section is focused on analysing the performance of the delay estimation algorithm.

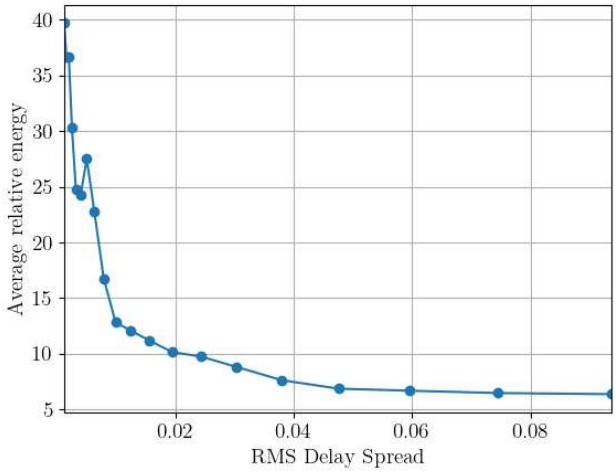

Figure 3.8: The ratio of orthogonality vs. RMS delay spread

In the process of estimating the channel frequency response across the 26 subcarriers in the discovery message, a ratio was taken between the energy of the integrated hypothesized modulated signal having the higher energy level to the energy of the signal with lower energy at the output of the matched filter. A trend for this ratio of orthogonality highlighting the relative energy of the two integrated hypothesized modulated signals is plotted against its respective RMS delay spread and presented in figure 3.8.

It is observed that with an increasing delay spread, this ratio gradually decreases from 40 to about 5.6.This is essentially a comparison of the relative strength of the symbols. This serves as a good insight into the energy disparity between the stronger and the weaker symbol at the output of the matched filter highlighting its decision threshold. A high energy ratio could imply a better detection and more reliable symbol recovery as well be indicative of a properly modulated signal. Apart from an insight into the quality of algorithm or modulation, the orthogonality ratio provides valuable insights into the channel conditions with a higher ratio being suggestive of a more stable channel condition with relatively low distortion. At a lower RMS delay spread, as can be seen from the figure presented, appropriately modulated signals are less likely to be impacted by the effects of spreading and multipath, thereby dominating the output during a matched filter decision. Following that, a decreasing ratio indicates that the quality of the received signal is deteriorating as the RMS delay spread increases. The presence of interference and noise caused by multipath propagation has negatively impacted the accuracy of signal detection and demodulation. This can lead

to errors in decision making, impacting the reliability of the communication system. The higher the ratio, the more the signals components are above the noise floor.

The approach introduced for the estimation of RMS delay spread for an unknown channel using both, time domain and frequency domain information involves correlating the statistical properties of the channel frequency response estimates with its multipath behaviour. It involves leveraging a wide-range of channel behaviour information which provides a comprehensive understanding of the channel of interest. It is a relatively simple approach of estimating the delay spread of the channel without requiring any channel impulse response measurements. It also eliminates the requirement of obtaining instantaneous channel data for adaptive systems by averaging the channel behaviour across a wide range of scenarios. This enables an adaptive system to correlate to different channel types, propagation environments, and multipath conditions, making it suitable for channels with diverse behaviors.

3.4 Estimation of Doppler Spread

In this section, how the Janus preamble can be used to extract an estimate of the Doppler shift and Doppler spread is presented. First, a description of the doubly spread wide-band channel model is introduced. Consecutively, the algorithm used for estimating the Doppler spread in the channel is described. Finally, the performance metrics for the estimator is presented.

3.4.1 Modelling of a Doubly Spread Channel

Time variability in a channel can arise either from inherent changes in the propagation medium or due to relative motion between the transmitter and the receiver. Changes that are inherent to the aquatic medium (change in temperature, salinity, etc.) occur over a wide period of time and do not impact the communication signals on an instantaneous level. However, the motion or surface waves resulting from winds or movement of vessels cause displacement of the reflection point for the signals resulting in a changing path length giving rise to scattering and Doppler spreading. The resulting Doppler effect can be represented as a time compression/dilation of the signal that causes frequency shifting and bandwidth spreading/shrinking [38]. If v is the relative velocity between the transmitter and the receiver,

c is the speed of transmitted waves, then the Doppler factor, a can be given as

$$a = \frac{v}{c} \tag{3.21}$$

The Doppler factor, a is proportional to the frequency distortion of acoustic waves under water. However, it is much more extreme in an UWA communication due to the slower speed of sound in water as compared to the speed of light in radio communications.

First, considering that a channel has only a single propagation path and a relative velocity of v_p between the source and the receiver, the corrected or estimated path delay, $\hat{\tau_p(t)}$, given that v_p is constant over t, can be mathematically represented as,

$$\hat{\tau_p}(t) = \tau_p(t) + a_p(t)t \tag{3.22}$$

where, $\tau_p(t)$ is the actual path delay and the term $a_p(t)t$ is the rate of change of the path delay for a path p with respect to time t. It accounts for the relative velocity v_p between the source and the receiver. Thus, $\hat{\tau_p(t)}$ is an estimation of the path delay at time t, taking into account the constant relative velocity and the change in path delay caused by that velocity.

But, in real world scenarios, the channel is made up of multiple propagation paths that can be grouped into clusters based on similarity in characteristics due to coming from the same path or reflecting off of similar surfaces. Each of these clusters are made up of multiple rays of signals that arrive at different points in time. If the channel is made of P clusters and each cluster is made of k signal paths, the channel frequency response, H can be mathematically modelled as a function of time and frequency as,

$$H(t, f) = \sum_{P=1}^{P} \sum_{k=1}^{k} h_{P,k} e^{j2\pi f \hat{\tau_p}(t)} \tag{3.23}$$

Expanding equation 3.23 using the mathematical equation in 3.22, H can be re-written as:

$$H(t, f) = \sum_{P=1}^{P} \sum_{k=1}^{k} h_{P,k} e^{(j2\pi f(\tau_p(t) + a_{P,k}t))} \tag{3.24}$$

Equation 3.24 with respect to the complex exponential, can be further simplified to:

$$H(t, f) = \sum_{P=1}^{P} \sum_{k=1}^{k} h_{P,k} e^{j2\pi f \tau_p(t)} e^{j2\pi f a_{P,k}(t)t} \tag{3.25}$$

where $a_{P,k} = v_{P,k}/c$

In equation 3.25, the term $h_{P,k}e^{j2\pi f\tau_p(t)}$ is a representation of the large-scale decaying gain multipath arrival and the term $e^{j2\pi f a_{P,k}(t)t}$ accounts for Doppler spread. The Doppler effect is evident from the shift in frequency given by the term $fa_{P,k}$ and a time-scaling factor given by μ where,

$$\mu = (1 + a_{P,k}) \tag{3.26}$$

3.4.2 Doppler Estimation

To estimate the Doppler shift, first, as described in [39], an auto-correlation on the signal is used on the input buffer to get the time scaling factor responsible for inducing time dilation. It is given by,

$$\mu = (1 + v/c) \tag{3.27}$$

The signal can then be resampled by a factor $1/\mu$ to compensate for the large scale Doppler.

Then, after down-conversion, the received signal is multiplied by the conjugate of the transmit signal, and the Doppler spectrum is obtained using the Welch approximation. The complex conjugate multiplication effectively shifts the frequency components of the received signal into the baseband, aligning them with the original transmit frequencies. If the transmit signal is given by, $x(t)$ and the received signal is given by $y(t)$, the resultant signal, $s(t)$ can be given by,

$$s(t) = y(t)x^*(t) \tag{3.28}$$

$s(t)$ is a measure of the correlation between the received signal and the complex conjugate of the transmitted signal, $x^*(t)$, which essentially provides information about the presence and alignment of the transmit signal within the received signal at different time instants.

The Welch approximation is particularly known for its ability to compute power spectral densities (PSD) with accuracy for time-varying or non-stationary signals. It computes the PSD by dividing the data into overlapping segments, computing a modified periodogram for each segment and averaging these periodograms to get a smooth average of the PSD. The Welch method's estimation equation for the PSD at a given frequency f for a signal, $s(t)$ can be given as:

$$PSD(f) = \frac{1}{N_{avg}\Delta f}\sum_{i=1}^{N_{avg}} |S_i(f)|^2 \tag{3.29}$$

where, $|S_i(f)|$ is the FFT of the $i-th$ segment at frequency f and N_{avg} is the number of

segments averaged that fits into the $s(t)$ after considering the overlap of 128.

$$\Delta f = \frac{F_s}{N_{FFT,DS}} \tag{3.30}$$

Here, $N_{FFT,DS}$ determines the number of samples per segment that are used for calculating the power spectral density (PSD). It affects the PSD resolution and the averaging estimate. The frequency resolution Δf obtained is 11.72 Hz. The value of $N_{FFT,DS}$ is chosen to be 2048 accordingly to achieve a trade-off between the frequency resolution and time resolution. Very high frequency resolution can come at expense of temporal localization of signal features or result in spectral leakage.

The Doppler spread that results from various vessel speeds ranging from 2 knots to 30 knots is recorded in steps of 2. In this work, the algorithm to estimate the Doppler spread is evaluated assuming a rich scattering environment in which the multipath arrival is lumped into a signal bin arrival. The number of path arrivals is limited to 30 to respect the central limit theorem and create a circularly complex Gaussian fading channel. The PSD data at each of these speeds are recorded along-with the corresponding vessel speeds which are then recorded to determine the frequency range over which the power is significantly concentrated to calculate the Doppler spread of this range. The PSD results are first converted into decibels and the minimum and maximum value for the PSD in dB are isolated. Subsequently, to estimate the Doppler spread, the frequency at which the PSD drops by 10 dB relative to the maximum value is computed using a Boolean that indicates whether the frequency at each index is within the in-band region. Finally, the value of the Doppler spread, D_s is given as,

$$D_s = \frac{D_{s,max} - D_{s,min}}{2} \tag{3.31}$$

The estimated results give an insight into the rate at which the frequency components of the signal are spreading due to the vessel's motion in a multipath underwater environment.

The Doppler spread estimation algorithm essentially analyzes the behavior of Doppler spread in a multipath channel as a function of vessel speed. It is run for the frame defined in the Aquatron experiments. The window size is tested for different frame lengths.In the estimation process, the FFT window, usually smaller than the length of the entire signal, was chosen to capture localised Doppler shifts within the signal. Three different window sizes, hereby referred to as, $W_{FFT,DS}$, have been used in the Doppler Spread estimation process to exhibit their performances, these being 16,384, 65536 and 262,144 equaling to

0.68 seconds, 1.36 seconds and 10.9 seconds respectively. The total window size, $W_{FFT,DS}$, could potentially affect the reliability of the spectrum.

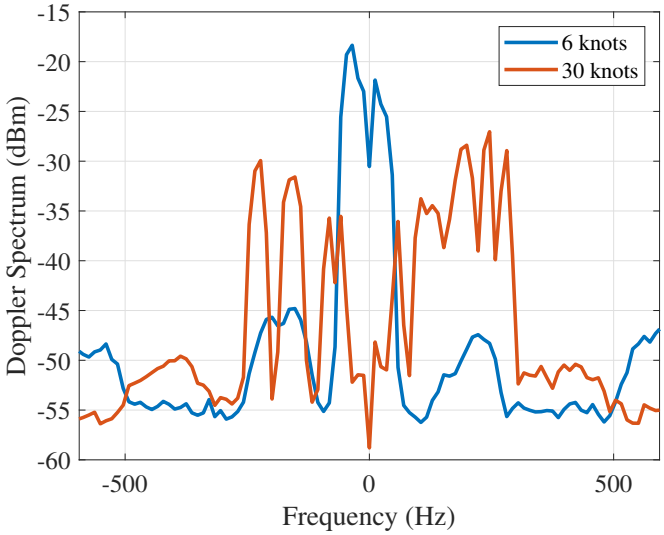

Figure 3.9: Doppler spectrum for different relative speeds.

The results of the Doppler spread estimation algorithm are shown in Figure 3.9, specifically, the Doppler spectrum. This plot presents the resultant Doppler spectrum in decibels (dBm) against frequency for two distinct vessel speeds, namely 6 knots and 30 knots. The plot compares the spectra at these speeds, highlighting the impact of vessel velocity on the channel's Doppler characteristics. This signifies that as a vessel accelerates, the channel's multipath-induced frequency dispersion becomes more pronounced. This analysis not only enhances the understanding of the dynamic nature of UWA channel in mobile scenarios but also provides valuable insights for the design and optimization of communication systems in vehicular and maritime environments.

3.4.3 Performance metrics for Doppler estimation

The performance of the Doppler spread estimation algorithm is presented in this section. It is a quantitative measure of how the estimation algorithm tracks and measures the frequency shift and spread in a given communication channel and it is pivotal in building confidence in the algorithm's accuracy and reliability.

Figure 3.10 present two different plots 3.10a and 3.10b for the estimated Doppler spread vs. the various vessel speeds from 0 knots to 30 knots for two different RMS delay spread

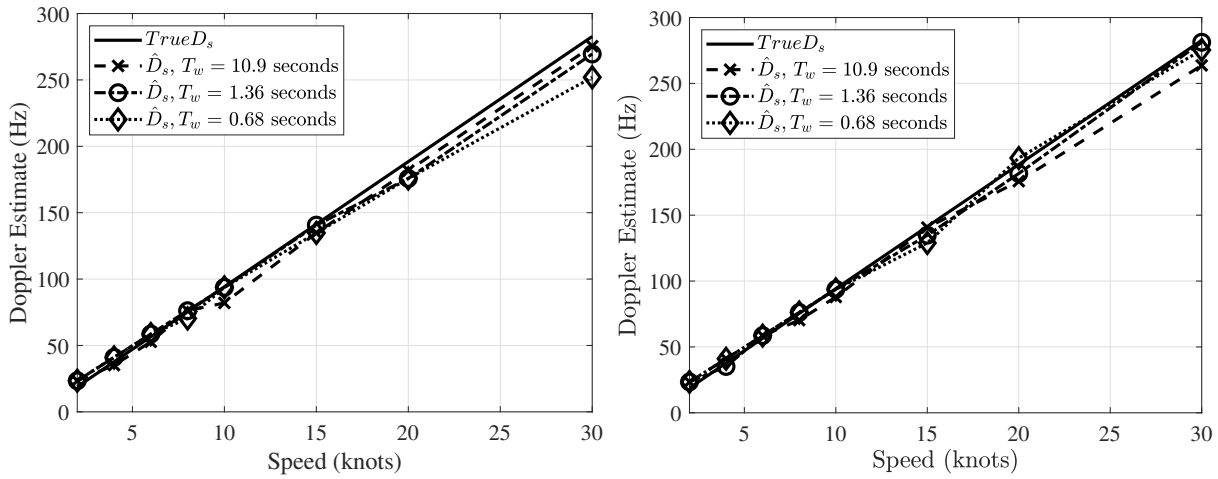

(a) Estimated Doppler spread for RMS delay spread of 8.3ms

(b) Estimated Doppler spread for RMS delay spread of 10ms

Figure 3.10: Doppler Spread estimates against true Doppler Spread for larger delay spreads

of 8.3 ms and 10 ms. The Doppler spread estimates are plotted along-with the theoretical Doppler spread prediction based on the vessel speed. The theoretical or true Doppler spread TD_s can be represented as:

$$TD_s = \frac{v_{knot}}{0.514cf_c} \tag{3.32}$$

where, v_{knot} represents the speed of the mobile vessel in knots, f_c denotes the carrier pass-band frequency at 27.5 kHz and 0.514 is the knot to metric system conversion factor. The Doppler Spread estimates for three different window lengths, $W_{FFT,DS}$, are introduced within the same plot for a comparison of their respective performances. Comparing the theoretical expectations to the estimated results reveals the degree to which the observed Doppler spread matches the theoretical predictions.

As is presented in the figures above, the estimated results follow the theoretical prediction values. This not only provides an evidence of the strong correlation between Doppler spread and vessel speed within this multipath channel but also signifies the robustness and accuracy of the Doppler estimation algorithm. The close agreement between the observed results and the theoretical expectations indicates that the dynamic effects of vessel motion on the channel's frequency dispersion has been effectively captured and quantified, thereby reinforcing confidence in the reliability of the analysis.

Figure 3.11 provides a comparison between two different threshold values of 3 dB 3.11a

and 10 dB 3.11b in the in-band calculation process for the Doppler spread estimation calculations.

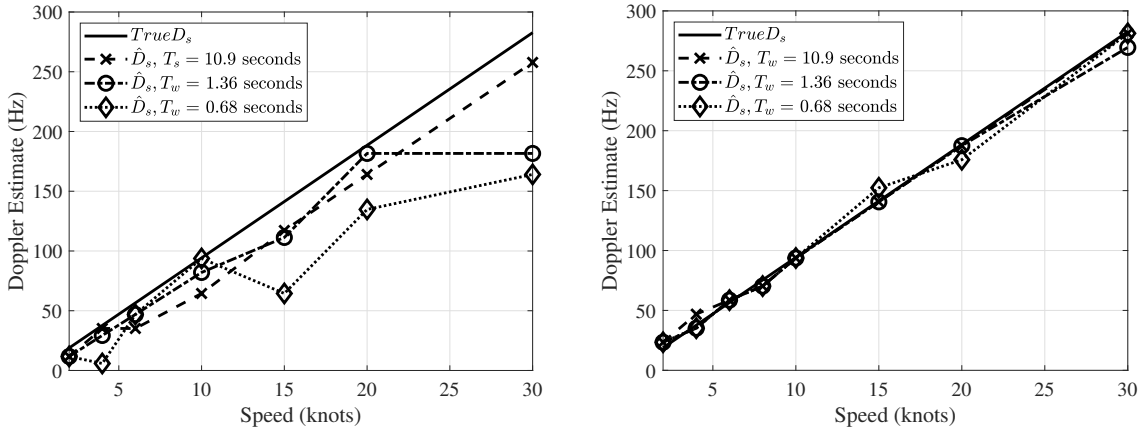

(a) Estimated Doppler spread for RMS delay spread of 0.3ms and 3 dB threshold

(b) Estimated Doppler spread for RMS delay spread of 0.3ms and 10 dB threshold

Figure 3.11: Performance metrics for Doppler Spread estimate against true Doppler Spread for different threshold values

As is imminent from the results in Figure3.11, 3 dB threshold provides a very rough Doppler spread estimate with respect to 10 dB. This can be attributed to the fact that 3 dB is more sensitive to fluctuation in the PSD and only captures a narrower band of frequencies around the peak PSD value thereby providing a more localised estimate. Although, an appropriate choice for narrowband frequencies, it captures minute variations and noise potentially affecting the accuracy of the Doppler spread estimation. In contrast, a 10 dB threshold proves to be more robust against smaller variations and noise around the peak frequency. However, it could end up potentially excluding relevant frequency components in the estimation. The choice in a threshold value has to be a well-informed trade-off between sensitivity and robustness based on the application and requirements.

The performance analysis allows for a direct comparison between the algorithm's outcomes and theoretical expectations thereby reinforcing the validity of the algorithm's underlying principles and mathematical foundations while also presenting a foundation of the algorithm's merits and weaknesses. The estimation process can be adapted to various vessel speeds, making it suitable for a wide range of applications where the speed of the source or receiver can vary significantly while also enabling for more accurate modeling compared to purely theoretical methods. However, the model banks on making proper decisions with

regards to threshold values, and FFT windows and Welch approximation segments. The accuracy of these assumptions could have potential implications on the results.

3.5 Estimation of Signal to Noise Ratio

In this section, the approach followed for estimation of the Signal-to-Noise ratio (SNR) is presented. In the process of modelling a communication link for simulation and analysis, introducing Additive White Gaussian Noise (AWGN) is imperative to replicate the real-world noise across communication channels which are rife with various sources of noises, including thermal noise, marine life sounds, and reverberations from shipping, mining and other extraction activities.

In the simulated channel model, SNR ranging from 0 dB to 40 dB was introduced in the channel for subsequent estimation at the receiver. To replicate the effects of AWGN, the noise power based on the chosen SNR level was calculated to generate random Gaussian noise samples with a uniform distribution. This noise, $n(t)$, was added to the transmitted signal, $x(t)$, in the channel to yield a received signal, $y(t)$,

$$y(t) = x(t) + n(t) \tag{3.33}$$

At the receiver, the SNR is estimated. First, the transmitted discovery message, which is considered known by the entire system is subtracted from the received signal. This isolates the noise, from the received signal.

Consecutively, the power of the estimated noise is calculated for the SNR estimation using

$$SNR = \frac{\int_{-\infty}^{\infty} |x(t)|^2 dt}{\int_{-\infty}^{\infty} |y(t) - x(t)|^2 dt} \tag{3.34}$$

But for real-world communication systems, the transmitter signal power cannot be considered for calculating or estimating the SNR of the received signal. This requires that the noise power be estimated from a portion of the received signal which is free of any waveforms or signals.

Combining equation 3.33 and 3.34, the linear SNR can be presented as

$$SNR = \frac{\int_{-\infty}^{\infty} |x(t)|^2 dt}{\int_{-\infty}^{\infty} |n(t)|^2 dt} = \frac{P_x}{P_n} \tag{3.35}$$

The dB value of SNR, as obtained from equation 3.35 can, thus, be presented as

$$SNR_{\text{dB}} = 10 \cdot \log_{10}\left(\frac{P_x}{P_n}\right) \tag{3.36}$$

where, P_x and P_n is the power of the transmitted signal and noise in dB respectively.

Utilizing the matched filtering algorithm for the demodulation and decoding of the received signal, the Bit Error Rate (BER) was computed across the entire range of Signal-to-Noise Ratios (SNR) spanning from 0 dB to 32 dB. Remarkably, the BER consistently registered at zero for all SNR values within this range.

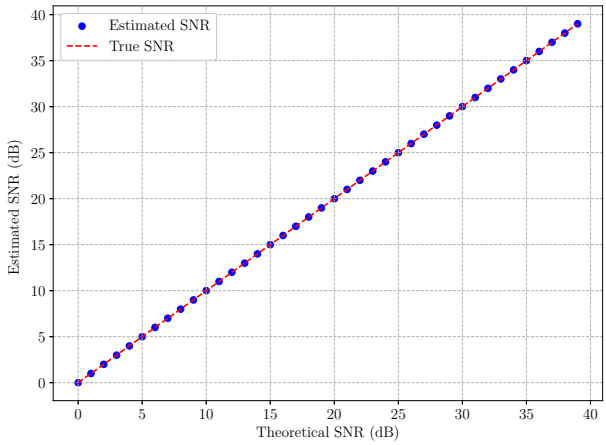

Figure 3.12: Plot overlaying estimated SNR against true SNR

The estimated SNR at the receiver has been plotted with respect to the theoretical values of SNR to compare the estimated values and the true values. The result of comparison is visualised in Figure 3.12. The results show that the estimated values overlap the true SNR values over a pure AWGN channel over 0 dB to an SNR of 40 dB with a mean squared error value of $2.7e^{-5}$.

When the signal passes through the propagation channel, it experiences path loss, fading, interference, and other effects that can modify its power. Additionally, the power amplifier at the transmitter side introduces amplification and potentially non-linear distortions. Due to these transformations and variations, the transmit and receive powers may not be directly comparable or in the same units when dealing with measured data-sets. Therefore, a correction factor or adjustment is typically needed to properly estimate the noise power. To estimate the noise power for measured data, the power in a noise-only period on the received signal is calculated as the transmit signal power is no longer reliable. The power of this

noise-only period is then subtracted from the noise of the received signal to account for the signal power.

While the estimation of channel SNR may seem to be of little importance in the proposed adaptive communication link, it is of paramount relevance given its role in the overall system performance. Even in scenarios where the RMS delay spread and Doppler spread plays a dominant role, a good SNR estimation can prove pivotal in selecting the best out of the available choices in adaptive modulation and coding while also maintaining a target BER, thereby balancing throughput and reliability.

In this chapter, the various techniques and algorithms implemented for the estimation of RMS delay spread, Doppler spread and, finally, SNR in UWA channel environments have been discussed in detail. The results obtained can serve to be the foundational tools to estimate the channel conditions of a real-world underwater acoustic channel to make informed decisions regarding important system parameters, such as modulation ratios, sub-carrier lengths, and guard band spacing for an adaptive system. In the subsequent chapter, these techniques have been implemented on real-world measured set of data that was recorded in the Aquatron Pool and the obtained results have thus been presented.

Chapter 4

Channel Characterisation using Measured Data

In this chapter, we analyze a dataset obtained from experiments conducted at the Aquatron facility, located at Dalhousie University in Halifax, Nova Scotia. The dataset includes measurements from the discovery message, and we examine its performance in characterizing an underwater channel.

4.1 Experimental Set-Up and Parameters

A trial at the Aquatron Laboratory, Dalhousie University Life Sciences Center, Halifax, Nova Scotia, Canada, was conducted to test the transmission of a frame for adaptive communication systems. Amongst the frames transmitted successfully during the course of this trial were frames transmitted to ensure calibration of equipment and a discovery message with multi-carrier modulated data and two Linear Frequency Modulated (LFM) frames. The objective of the experiment was to transmit a set of frames that can be used to characterise an adaptive communication system.

The frames transmitted for the channel characterization of an adaptive communication system consists of two LFMs followed by a 10-second Frequency Hopped Binary Frequency Keying (FH-BFSK) modulated convolutional encoded PN Sequence and OFDM symbols of varying symbol size of the order 2N where N = 5,6,7. The FH-BFSK modulated portion of the transmission frames were designed to combat the high delay spread within the Aquatron Pool with a symbol period of 1 millisecond. Three exact and consecutive frames were transmitted at a time. The table 4.1 presents the various parameters used in the design of the FH-BFSK discovery frames for the Aquatron Pool trial.

The signal generator and the transmission set-up is represented by a flow-diagram in Figure 4.1. A DC Power supply is used to power the power amplifier (PA) and an appropriate voltage within the range of 40V to 44V (max) is supplied. A C-programming based code triggers the transmission of the wave files located in the SD Card of the Zybo Z7-10 FPGA board. This FPGA board is attached to a pre-amplifier 3rd order low-pass filter. The

Table 4.1: Parameter specifications for the discovery message for Pool Trial

Parameter	Value
Carrier Frequency	-96 Hz, 96 Hz
Passband Frequency	27.5 kHz
Bandwidth	5 kHz
Clock Frequency	96 kHz
Oversampling rate	1000
Symbol period	10 msec
Frame duration	21.3 sec

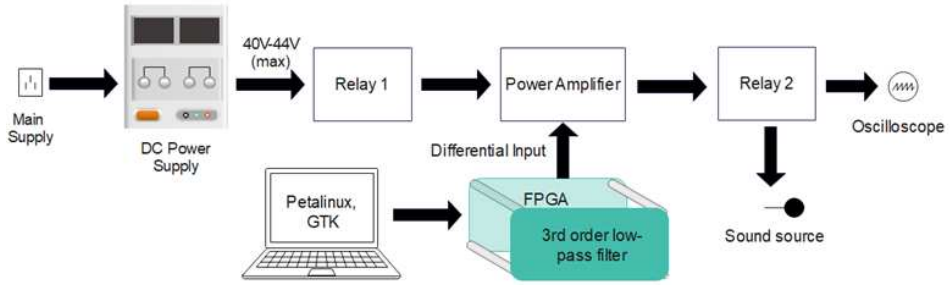

Figure 4.1: A flow diagram representing the signal generator set-up at the transmitter

waveforms amplified by the PA are sent to the signal source. An oscilloscope was used to continuously tracks the waveforms being transmitted in real time.

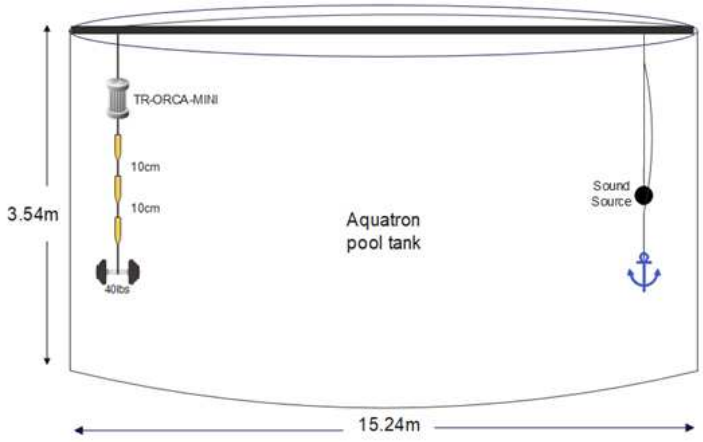

Figure 4.2: A diagram representing the transmitter and receiver positioning inside the Aquatron Pool tank

The experiment was conducted in the Aquatron pool tank which boasts of a diameter of 15.24m and a depth of 3.54 m on the edges to 3.91m at the center. It houses 684,040

liters of unfiltered seawater and a hydraulically controlled bridge spanning its diameter along which the transmitter and receiver hydrophones were hung with appropriate anchors. The signal generation equipment was placed at one end of the bridge and cabled to the sound source by a 5m long cable. The transmitter sound source used for this experiment was a Benthowave BII-7522 with a transmitting voltage response (TVR) of 155 dBm Re 1μPa/V at 1 m from the source. It was therefore crucial to place the transmitter and receiver with enough distance between each other to avoid receiver saturation.

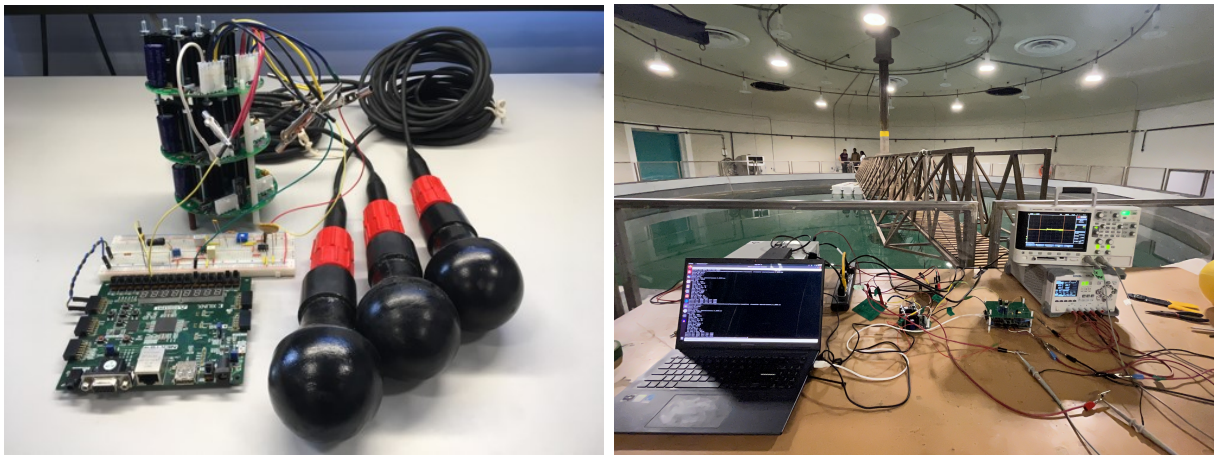

(a) Transmitter circuit with transducer hydrophones

(b) Experimental set-up at the Aquatron Laboratory

Figure 4.3: Experimental Setup and Equipment Used

The receiver was operated through the TR-ORCA-MINI with synchronously sampled hydrophone inputs that is capable of capturing, recording and streaming underwater acoustic data sets in real-time. It was configured with three hydrophone inputs to record data over three channels at 96 kSps. The receiver was deployed with three hydrophones at the other end of the pool directly across the diameter from the signal generator. The relative position between the transmitter and receiver is presented in Figure 4.2. The receiver hydrophones were separated from each other by a distance of 10cm or by $\lambda/2$. Given in Figure 4.3 is the set-up for the entire experiment including the equipment used.

4.2 Characterising the Channel in Calm Water Condition

In this section, the measured set of data obtained from transmitting the discovery message in a relatively still water at the pool is analysed and the channel under these conditions are

predicted with respect to RMS delay spread and Doppler Spread.

In each transmission, three consecutive and similar frames were employed. Multiple such transmissions were conducted, varying in location and signal power. For channel characterization, a transmission in a relatively calm water condition with a non-saturating signal amplitude at the receiver was selected. All three frames within this transmission were subject to analysis.

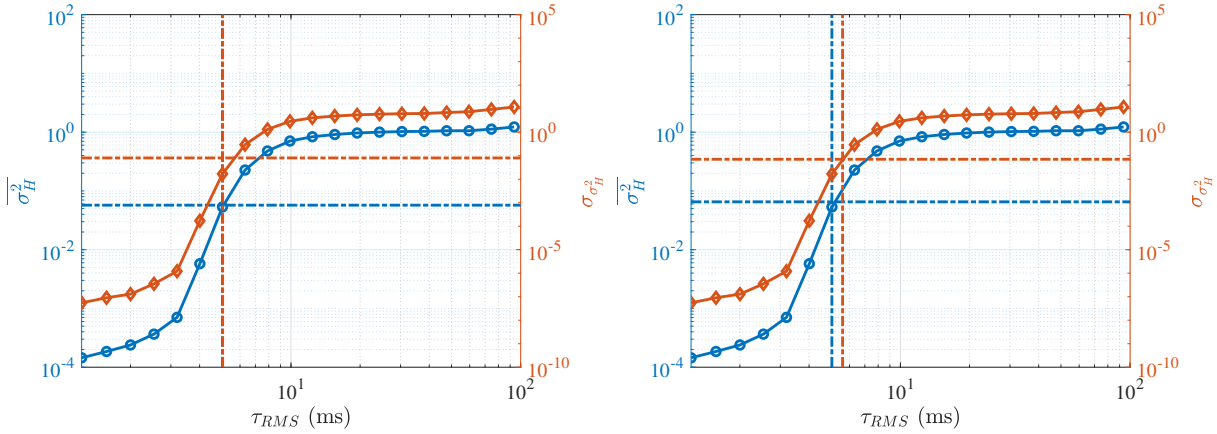

(a) Channel mean and standard deviation vs. RMS Delay spread for first frame

(b) Channel mean and standard deviation vs. RMS Delay spread for second frame

(c) Channel mean and standard deviation vs. RMS Delay spread for third frame

(d) Channel statistics vs. RMS Delay spread averaged over three frames

Figure 4.4: RMS Delay Spread Estimation using channel statistics

To begin, each of these three frames were isolated for separate post-processing and analysis. They were then filtered, down-converted, and subsequently re-filtered to eliminate ambient and environmental noise. Synchronization with the transmitted data was achieved

through a sliding window approach, which determined the optimal cross-correlation point between the transmitted and received frames. Following synchronization, frequency-dehopping and demodulation were performed. The channel frequency responses were recorded, and calculations were made for mean variance and standard deviations. Bit error rates were then computed, both for coded and uncoded data. To extrapolate the channel's RMS delay spreads, the obtained mean and standard deviation values were marked on a generalized plot for a multipath model. This plot featured varying levels of multipath in relation to their respective RMS delay spreads, as previously described in Chapter 3. The results obtained for Frames 1, 2, and 3 along with an averaged result is presented in Figures 4.4a, 4.4b, 4.4c and 4.4d. The RMS Delay spread of the channel as obtained from the three frames and an average of the three frames are presented in Table 4.2

Table 4.2: Estimated RMS Delay Spread values for a relatively still UWA channel

Frame	Estimated RMS Delay Spread
Frame 1	5.03 ms-5.04 ms
Frame 2	5.03 ms-5.6 ms
Frame 3	5.03 ms-5.7 ms
Average of Frame1, 2 and 3	5.03 ms-5.6 ms

The analysis of RMS delay spreads for three consecutive transmission frames, along with an averaged RMS delay spread computed over these frames, reveals that the estimated channel delay spread lies in between 5.03 ms to 5.6 ms. Each of the three frames consistently exhibits a lower limit of 5.03 ms, while the calculated average delay spread of 5.6 ms for the upper limit reinforces the confidence of the estimation results. These results further indicate the presence of short multipath components. These insights can prove vital for optimizing communication systems to allow for effective management of multipath effects and ensuring reliable underwater communication performance. By utilizing the transmitted Linear Frequency Modulation (LFM) signals before the Frequency Shift Keying (FSK) frames, the Root Mean Square (RMS) delay spread was determined to be approximately 4.0 ms. In contrast, the proposed technique yielded a value of 5.06 ms. Although these values indicate relatively similar multipath characteristics, the slight disparity suggests that the proposed technique has the potential to capture subtle propagation behavior of the channel.

In the stable multipath environment without any wave presence, the signal-to-noise ratio (SNR) of the channel was estimated using the technique described in Chapter 3. First,

the noise density was determined by analyzing a portion of the received data frame that contained no signal, representing a waveform-free space. Subsequently, the average noise power was computed and subtracted from the overall received signal, yielding the signal power. The calculated SNR value was determined to be 19.75 dB.

The transmission of FSK was preceded by two LFMs solely for the purpose of synchronisation. The LFM based synchronisation and corresponding cross-correlation between the transmitted and received signal revealed a very high multipath channel with 3 distinct path of arrivals in the channel impulse response 4.5a and a channel delay of 0.08 seconds. When a model with varying SNR for a channel impulse delay of 0.08 seconds was simulated, the BER started getting worse as SNR grew higher than 24 dB as presented in Figure 4.5b. As a result, BER was no longer used as a performance metrics for the transmission of the frames under these channel conditions. Instead, a ratio-of-orthogonality for frame 1, frame 2 and frame 3 was calculated to evaluate the estimation algorithm's performance.

As was described in Chapter 3, section 3.3.4, the ratio of orthogonality provides a much better insight into the channel conditions as well as the performance of the decision algorithm in the face of unknown channel characteristics. The calculated ratio of orthogonality for all the three frames, suggesting the relative energy between the hypothetical symbols before the algorithm's decision making step is given in table 4.3.

Table 4.3: Ratio of orthogonality for all three frames

Frame	Ratio of Orthogonality
Frame 1	10.71
Frame 2	9.73
Frame 3	9.37

Based on Figure 3.8, it can be observed that a modelled system with an average Signal-to-Noise Ratio (SNR) of 25 dB indicates that in a multipath channel with an RMS delay spread exceeding 2 milliseconds, the orthogonality ratio decreases from 40 to 5.6. This reduction in orthogonality implies that symbols experience spreading due to the adverse effects of severe multipath propagation. Consequently, the accuracy of a matched filter-like algorithm in establishing a distinct decision boundary is compromised.

Nevertheless, considering that the average relative energy for the three frames remain close to 10, it is suggestive that despite significant spreading caused by channel effects, the algorithm exhibits better-than-average performance during the decision-making process

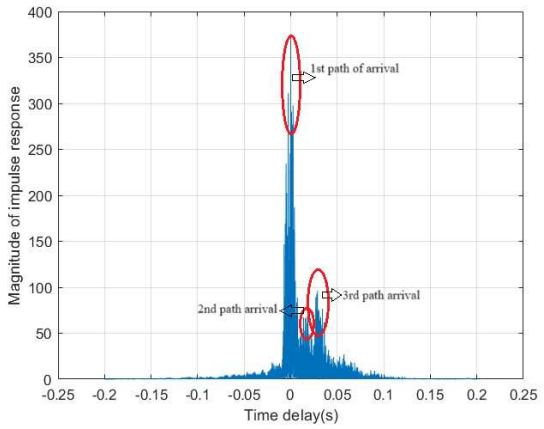

(a) The Channel Impulse Response of the Aquatron channel estimated using an LFM

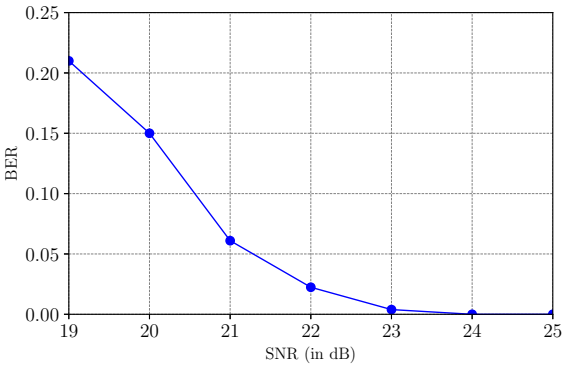

(b) The BER vs. SNR for a multipath model with a delay of 0.08 seconds

Figure 4.5: CIR and BER modelling for a multipath of 80 milliseconds of channel delay

in channel estimation. As a result, the statistical characteristics of the channel can be considered reliable.

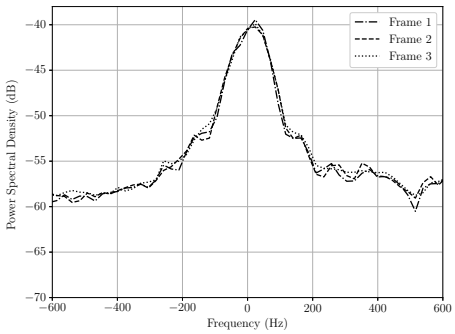

(a) Doppler Spectrum of all three frames using Welch approximation

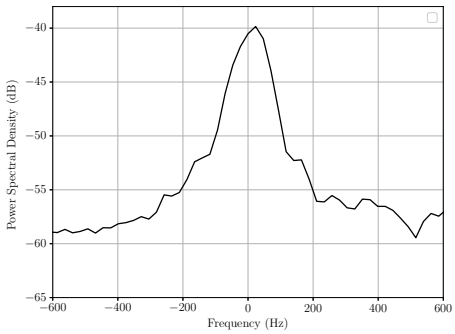

(b) Average Doppler Spectrum of all three frames using Welch approximation

Figure 4.6: Individual frame Doppler spread and average Doppler spread of a wave-free multipath channel

The Doppler Spectrum is estimated using the Welch approximation. The received signal and the complex conjugate of the transmitted signal over an FFT window of 4096 points have been used to estimate the Doppler spread spectrum for all three transmitted frames. A frame window size of 262144 or 5.45 seconds is used for obtaining the PSD of the data set. Their Doppler spectrum have been plotted in Figure 4.6a. Consecutively, the Doppler Spread obtained for the three frames using the 3-dB points in Welch approximation method

are presented in Table 4.4. An average of the power spectral densities from the three frames is used to find an average Doppler spread of the channel as is presented in 4.6b. The estimated Doppler Spread values vary across the three consecutive frames, indicating that the channel characteristics are not constant during this time period implied by a change in the transmitted signals over time.

Table 4.4: Estimated Doppler spread for individual frames and their average

Frame	Doppler Spread
Frame 1	93.5 Hz
Frame 2	100 Hz
Frame 3	96 Hz
Average of Frame 1, 2 and 3	99.27 Hz

However, it is necessary to note that a high RMS delay spread coupled with low SNR conditions cause a dispersion of multipath components in the channel, leading to considerable overlapping. This multipath dispersion can introduce time-varying frequency shifts and distortions, making it harder to estimate the Doppler spread accurately. The high delay spread has resulted in frequency-selective effects, which can further complicate the estimation process and estimate the Doppler Spread to be higher than its true value. To assess the impact of high multipath and low SNR conditions on the estimation of Doppler shift and Doppler spread in a given channel, a simulation was performed with a signal-to-noise ratio (SNR) of 25 dB and a relatively high root mean square (RMS) delay spread of about 100 ms. The results of the Doppler estimation indicated a shift that was considerably higher than the actual Doppler value. The combined effect of multiple signal components arriving at different phases and amplitudes along with noises and interference results in an increased apparent Doppler spread. The Aquatron pool, being a shallow and small pool, exhibits extremely high channel impulse delay of about 80 ms which is typically not encountered in a real world scenario. In actual oceanic environments, the presence of multiple strong and distinct reflection paths encountered in the pool is expected to be significantly reduced. Moreover, a clear line of sight (LOS) path between the transmitter and receiver is more likely to be available, allowing for a more direct and unobstructed signal propagation with a significant improvement in Doppler estimation performance.

To establish a performance benchmark for the Doppler spectrum estimation under ideal conditions assuming that the received signal is exact and identical to the transmitted signal,

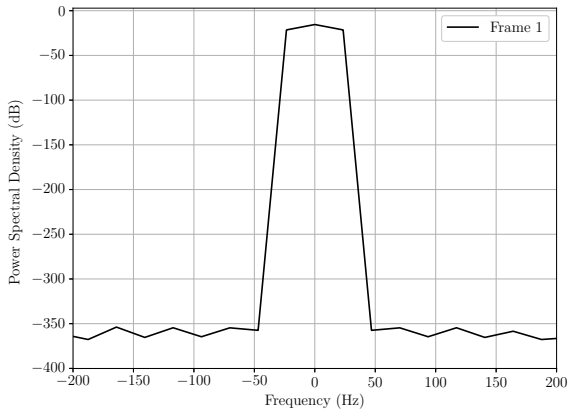

Figure 4.7: Doppler Spectrum assuming ideal conditions

the Doppler spectrum is obtained and presented in Figure 4.7. The results suggest that in the absence of any external factors, such as noise, interference, or other impairments, the channel is expected to exhibit a maximum Doppler spread of 50 Hz. This sets the achievable limit and allows for the evaluation of the system's performance relative to its maximum potential.

It is important to note that the results of the Doppler estimation in these channel conditions are physically not true as no waves were observed during these transmissions. This is suggestive of the requirement of more evolved Doppler estimation techniques in high multipath and low SNR channel environments. This could be an interesting scope for potential future work.

The Bit Error Rate calculated for both, coded and uncoded data, for all the three frames are presented in Figure 4.5. The notable enhancement in BER performance with the use of channel coding highlights the critical role of data encoding before transmission. The system consistently achieved a remarkably low BER across all three frames when coding was applied. These results highlight the effectiveness of error-correcting codes in mitigating transmission errors and enhancing data reliability. The occurrence of bit errors can be attributed to the combination of a high Signal-to-Noise Ratio (SNR) value of approximately 19 dB and the presence of a severe multipath channel with an RMS delay spread exceeding 5 milliseconds.

The decoding of the measured channel data utilized a Viterbi decoder with an enhanced decision depth of 20 bits. The increased decision depth allowed for a significant improvement in the bit error rate. As a result, the decoder considered a longer history of received bits

Table 4.5: Coded and Uncoded BER for all three frames

Frame	BER uncoded	BER coded
Frame 1	0.051	0.003
Frame 2	0.043	0.007
Frame 3	0.053	0.006

during the decoding process. This increased memory allowed for better error correction capabilities and improved the overall performance of the decoding algorithm. Increasing the decision depth in a Viterbi decoder can lead to a reduction in the accuracy of decoded bits near the end of the frame. Specifically, for a decision depth of n bits, n bits are lost from the end of the frame. The choice of decision depth involves a trade-off analysis and optimization process based on the particular application and system constraints. It may require iterative adjustments and fine-tuning to find the decision depth that strikes the best balance between accuracy and loss of bits for a given scenario. Considering this, it is suggestive that the ratio-of-orthogonality is a more informative metric in terms of providing comprehensive and statistically meaningful information about the channel conditions, compared to the BER.

4.3 Characterising the Channel in Wave-Infused Condition

To test the ability of the discovery message to characterise the Doppler Spread in a channel with significant amount of waves resulting in considerable frequency dispersion, a pontoon in the Aquatron pool was utilised to induce water surface disturbances and waves. In this section, the data sets obtained during the presence of these channel disturbances have been analysed and the channel characterisation results have been presented.

The estimated channel RMS delay spreads are presented in Figure 4.8 with each individual frame's channel statistics plotted against the RMS delay spreads. An average of the three frames is also used for a more generalised conclusion for the channel under wave-infused conditions. Table 4.6 provides the estimated RMS delay spread values for all three frames and the average RMS delay spread over these three frames under the given conditions. The channel delay spread is estimated to be between 5.9 ms to 6.9 ms. An analysis of all three frames indicated a consistent higher limit delay spread value close to 7.0 ms. This data can prove sufficiently important while designing a communication system equipped to combat the effects of multipath in an environment with rampant frequency dispersion. The RMS delay spread of this channel when calculated using the LFMs was found to be 4.8 ms.

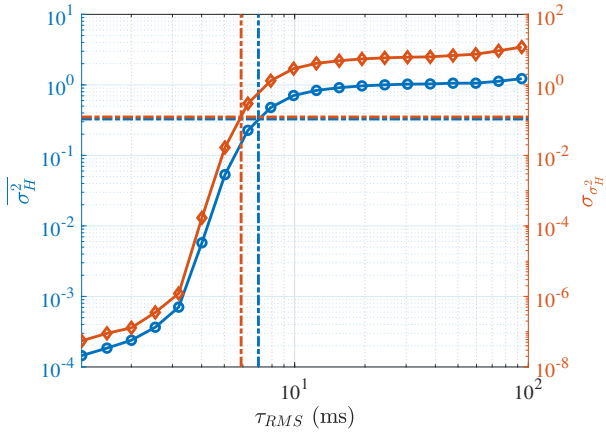

(a) Channel mean and standard deviation vs. RMS Delay spread for first frame

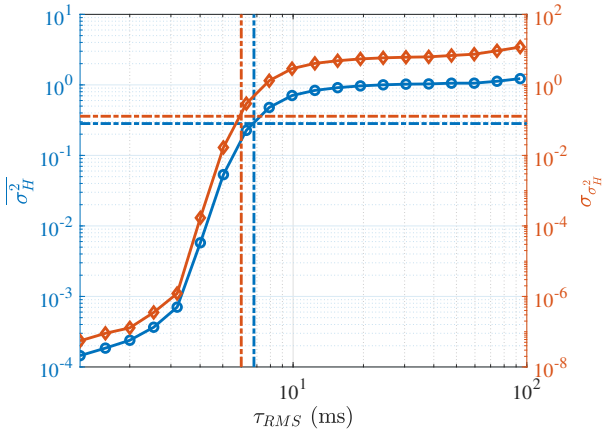

(b) Channel mean and standard deviation vs. RMS Delay spread for second frame

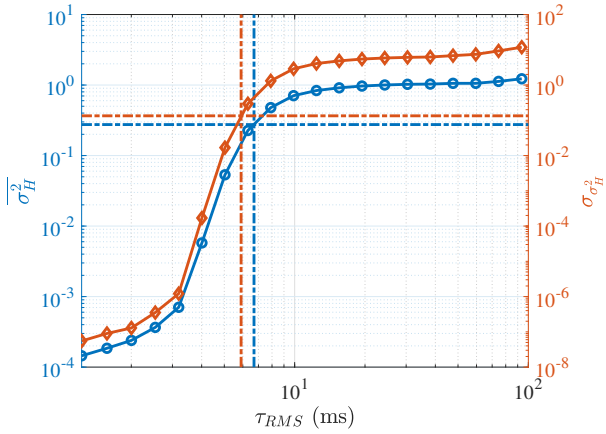

(c) Channel mean and standard deviation vs. RMS Delay spread for third frame

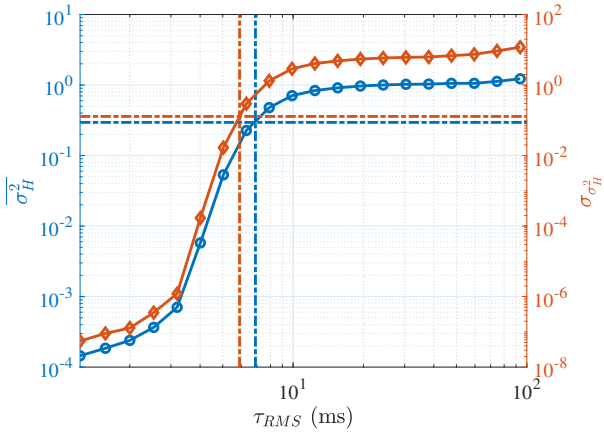

(d) Channel statistics vs. RMS Delay spread averaged over three frames

Figure 4.8: RMS Delay Spread Estimation using channel statistics for wave conditions

Table 4.6: Estimated RMS Delay Spread values for a UWA channel with waves

Frame	Estimated RMS Delay Spread
Frame 1	5.9 ms-7.0 ms
Frame 2	6.0 ms-6.8 ms
Frame 3	5.9 ms-6.7 ms
Average of Frame 1, 2 and 3	5.9 ms-6.9 ms

Table 4.7 displays the orthogonality ratio observed for the three frames transmitted through a channel affected by wave interference. The table illustrates the variations in channel conditions across the frames. The results indicate that the channel condition during the transmission of Frame 1 was notably worse compared to Frame 3. As the frames progressed,

the channel quality improved, evident from a higher ratio of relative energies between the hypothetical BFSK frequencies at the decision-making stage of the matched filter. This observation suggests a positive trend in the channel condition over time, with Frame 3 experiencing the most favorable channel conditions among the three frames. The increasing ratio of relative energies indicates a more distinct separation between the desired signal and the interference, leading to improved orthogonality and enhanced signal quality.

Table 4.7: Ratio of orthogonality for all three frames

Frame	Ratio of Orthogonality
Frame 1	7.73
Frame 2	10.05
Frame 3	11.61

The Doppler spreads calculated for a channel condition characterized by high wave activity revealed a consistent Doppler spread value across all three frames subjected to analysis. In this specific scenario, a Doppler spread varying between 95 Hz to 106 Hz was observed between the three subsequent frames, highlighting an overall consistency of the channel's frequency dispersion characteristics in the presence of significant wave-induced motion. Th Doppler spectrum's PSD plot is presented in Figure 4.9. The consistency in the estimated results for Doppler spread suggests that the channel's frequency dispersion characteristics remained remarkably stable even when subjected to pronounced wave dynamics. Such stability in the Doppler spread can potentially be a promising indicator for underwater communication systems, implying that the channel can maintain a relatively constant frequency response, thereby, facilitating the design of robust communication systems.

Table 4.8 displays the 3-dB threshold value of the Doppler spread for Frames 1, 2, and 3 in the presence of significant channel disturbances.

Table 4.8: Estimated Doppler Spread for an UWA channel with waves

Frame	Estimated Doppler Spread
Frame 1	102.4 Hz
Frame 2	95.2 Hz
Frame 3	106 Hz
Average of Frame 1, 2 and 3	103.2 Hz

The average Doppler spread in the wave condition (103.2 Hz) is slightly higher than in the wave-free condition (99.27 Hz). The presence of waves introduces additional frequency

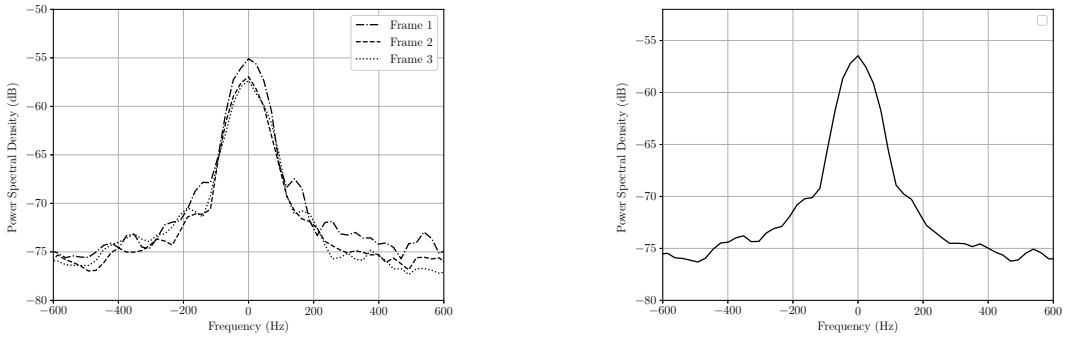

(a) Doppler Spectrum of all three frames using Welch approximation

(b) Average Doppler Spectrum of all three frames using Welch approximation

Figure 4.9: Individual frame Doppler spread and average Doppler spread for wave conditions in the multipath channel

variations to the channel. The wave-induced motion contributes to a larger Doppler spread, suggesting a more dynamic channel in the wave condition. The frequency variations caused by wave-induced motion can result in increased frequency selective fading and inter-symbol interference. However, the values for the two highly contrasting situation is very close to each other. This is because the propagation characteristics of the wireless channel, such as scattering, diffraction, or refraction, can also introduce frequency variations. Even in a wave-free condition, there can be small-scale variations in the channel due to these propagation effects. These variations may contribute to a higher Doppler spread than expected in the absence of visible waves. Furthermore, if there are objects or obstacles causing reflections or multipath propagation, it can result in additional frequency shifts and a larger Doppler spread. This calls for the need of more advaced Doppler Spread estimation techniques and algorithms to properly estimate channel Doppler in particularly harsh conditions.

As the transmission progressed from Frame 1 to Frame 3, there were noticeable changes in the channel characteristics. While the Doppler spread significantly worsened in Frame 3, there was an improvement in the delay spread of the channel. Specifically, the delay spread decreased from 7.0 msec in Frame 1 to approximately 6.7 msec in Frame 3. These changes in the channel properties had a direct impact on the orthogonality ratio. Despite the worsening Doppler spread, the improved delay spread contributed to an overall enhancement in the orthogonality ratio as the transmission progressed from Frame 1 to Frame 3. The reduced delay spread indicates a more focused and distinct separation between the multipath

components of the channel, leading to improved orthogonality and better signal quality. This improvement in orthogonality compensates to some extent for the increased Doppler spread observed in Frame 3, resulting in an overall positive trend in the orthogonality ratio throughout the transmission.

Table 4.9: Coded and Uncoded BER for all three frames

Frame	BER uncoded	Code Depth 10	Code Depth 15
Frame 1	0.0361	0.002	0.0
Frame 2	0.038	0.004	0.0
Frame 3	0.03	0.0	0.0

Table 4.9 illustrates the Bit Error Rate (BER) rates for both coded and uncoded data under the given channel conditions. The BER exhibited a noticeable trend of improvement as the transmission progressed from Frame 1 to Frame 3. In Frame 3, characterized by a relatively reliable channel condition, the coded data demonstrated exceptional performance with a BER of 0 for a small decision depth of 10 and beyond. This indicates a high level of accuracy and reliability in the transmission of the coded data. The observed improvement in the BER rates suggests that the channel conditions became increasingly favorable as the frames were transmitted. This trend highlights the impact of channel quality on the error rates and emphasizes the importance of reliable channel conditions for achieving low BER values. The trends in the BER closely align with those observed in the RMS delay spread and the ratio of orthogonality. This correspondence further highlights the reliability of the ratio of orthogonality as a performance metric for the devised estimation algorithms, even in the presence of a highly mobile channel. Moreover, when the bit depth of the Viterbi decoder is increased from 10 to 15, a significant improvement is observed in the bit error rate (BER), resulting in a perfect BER of 0 for all three frames. This finding implies that by striking a balance between the number of bits that can be sacrificed towards the end of the frame and the accuracy of the data, it is possible to achieve a well-balanced performance and reliable transmission of information.

The SNR estimation technique, described in Chapter 3, was employed to estimate the signal-to-noise ratio (SNR) for the channel under the infused wave condition. The estimated SNR was determined to be 15.27 dB, indicating a highly noisy channel environment. In such noisy channel conditions, it becomes crucial to employ effective techniques to mitigate the impact of noise and improve the reliability of the transmitted payload. For example,

proper power amplification to boost the signal power before transmission can enable sufficient compensation for the signal degradation caused by noise and other channel impairments.

A quick comparative analysis of both the wave free and wave-induced conditions suggest that as the wave-free condition exhibits a higher SNR compared to the wave-induced condition, indicating better signal quality and a potentially more reliable communication environment in the absence of waves. The wave-free and wave-induced conditions have similar ratios of orthogonality, suggesting comparable levels of interference and multipath effects in both conditions. This is in-line with the experiment as the position of the transmitter and receiver remained unchanged during the course of both types of transmission. In addition, the wave-induced condition exhibits a slightly higher RMS delay spread compared to the wave-free condition, indicating a wider spread of arrival times of multipath components. This suggests more severe multipath propagation effects in the presence of waves. The wave-induced condition also exhibits a slightly higher Doppler spread compared to the wave-free condition, indicating a larger frequency variation due to wave-induced motion. This suggests a more dynamic channel in the presence of waves.

In this chapter, both Doppler and delay spread estimation, accompanied by an evaluation of Bit Error Rate (BER) performance for coded and uncoded data have been introduced for acoustic signals recorded in real-world. These findings unveil various nuances of underwater channel behavior, serving as foundational knowledge for the optimization of communication systems. The primary objective of this exercise has been to decipher the underlying channel impairments in the Aquatron Pool and their dynamic nature, with the ultimate aim of leveraging this insight for the development of adaptive communication systems. Through a systematic examination of Doppler and delay spread behavior across a spectrum of scenarios, this endeavour has laid a foundation for informed decision-making in communication system design in this specific channel.

Chapter 5

Conclusion

In this chapter, a conclusion is presented. Specifically, in Section 5.1, the summary of contributions will be discussed, then in Section 5.2, the future work is addressed.

5.1 Summary of Contributions

In this work, the use of a Janus-like discovery message to estimate different channel characteristics is described. The fundamental premise in this research is the realization that an effective estimator, embedded within a JANUS-inspired discovery message, can serve as a cornerstone for channel-aware communication strategies. The proposed estimator can be used to inform the nodes in the communication network to optimize the physical layer parameters as well as upper layer network settings, allowing for dynamic adaptation and optimization of communication settings. It is demonstrated that a figure of merit quantifying the channel multipath and Doppler spread can be fed back between the receiver and transmitter. For the multipath, in this research, it was demonstrated that the CFR variation of the estimated narrowband channel amplitudes over the bandwidth has a strong intrinsic relationship with the RMS delay spread. A long message of 2048 symbols was meticulously designed to acquire comprehensive channel statistics. Furthermore, the utilization of this discovery message and a subsequent statistical analysis has allowed us to delve deeper into the intricacies of channel behavior.

The promising outcomes presented herein point to the potential for mitigating channel-related hurdles and ensuring the reliable transmission of data across varying conditions. The objective to enable future underwater communication systems remains, equipping them with the adaptability required to thrive in the face of the inherent complexities of underwater channels.

In this work, the effect of channel impairment such as Delay spread and Doppler spread on signal propagation in an underwater acoustic channel are carefully analyzed. To emulate these impairments, a multipath channel with exponentially decaying gain producing RMS

delay spreads between 0.3 ms to 100 ms was modelled. An algorithm very similar to a bank of matched filters was implemented at the receiver to estimate the channel frequency response of the received signal. The estimated channel frequency response was confirmed to be a match of the modelled channel. The channel statistics were then extracted from the estimated channel frequency responses for all 26 subcarriers. The mean and standard deviation of the channel frequency responses were used to estimate the channel delay spread. To simulate the surface waves induced by motion that gives rise to Doppler spreading, a range of vessel speeds, spanning from 2 knots to 30 knots, was employed. This comprehensive spectrum of speeds allowed for the replication of conditions for both mild and extremely high Doppler spreads. The 3-dB Doppler spread at the receiver was then estimated by evaluating the regrowth in the spectral line of the modulated data. These algorithms were tested on a set of data measured in the Aquatron's tanks. The transmissions were conducted in a condition with no waves followed by high wave conditions. The RMS delay spread and Doppler spread were estimated using the algorithms mentioned on three consecutive and similar frames for each of the channel conditions. This seeks to provide an enhanced confidence in the estimated results.

The utilization of a long discovery message as a channel discovery technique serves multiple purposes. Firstly, it is a crucial component in achieving an adaptive system. Additionally, it offers the advantage of transmitting a payload of 1024 bits while providing us with valuable channel-related data. These obtained channel data can be a valuable asset in the design of adaptive communication systems to improve overall system performance, such as increased data rates, better spectral efficiency, or enhanced reliability. By periodically monitoring the channel characteristics and adjusting transmission parameters accordingly, the system can mitigate the impact of fading, interference, and other channel impairments. In scenarios with challenging or dynamic channel conditions, adaptive optimization ensures robust and reliable communication. By dynamically adjusting parameters like modulation ratio, subcarrier length, and guard interval size, maximum bandwidth utilization can be achieved resulting in increased data rates and faster transmission. The acquisition and transmission of significant amounts of statistical channel data over an acoustic channel can, however, pose a considerable challenge due to its inherent latency. As a result, a potential trade-off emerges between the performance gains achieved through system adaptability and the complexity involved in implementing such a system. By leveraging the knowledge of channel data, such

as the RMS delay spread and Doppler spread, we can determine the optimal number of subcarriers needed to achieve a specific throughput. Conversely, if we have a system with a fixed number of subcarriers, we can estimate the feasibility of communication through the acoustic channel by calculating the expected throughput value. This information allows us to make informed decisions regarding the design and performance of the communication system. In scenarios where the potential gains in system efficiency and performance outweigh the additional complexity and associated costs of designing sophisticated algorithms for parameter optimization and adaptation, an adaptive system utilizing channel data can indeed be worth the trade-off. Alternatively, in situations where the complexity and costs outweigh the potential benefits, a simpler fixed-parameter system may be more appropriate.

5.2 Future Work

Some of the future avenues for this research could be deeper delve into refining the defined channel models to capture more nuances in underwater communication environments. Investigation of more complex scenarios, such as varying water depths, oceanographic conditions, and dynamic marine life interactions, can prove substantial in the development of comprehensive and adaptable channel models. Furthermore, an in-depth analysis could be performed to understand the impact of changing the length of each transmission symbol. Another subsequent phase of this research holds the potential for the development of an adaptive communication system, leveraging the acquired insights into channel behavior to incorporate an adaptive mechanism capable of seamlessly transitioning between multicarrier modulation and Frequency Shift Keying (FSK) in response to the prevailing channel conditions or enabling an more robust and reliable data transmission by modifying transmission parameters such as modulation ratio and subcarrier length and subcarrier spacing.

Bibliography

[1] Barbier E. et al Duarte C.M., Agusti S., "Rebuilding marine life," *Nature 580*, p. 39–51, 2020.

[2] J. B. et al Jackson, "Historical overfishing and the recent collapse of coastal ecosystems," *Science*, vol. 293, pp. 629–637, 2001.

[3] D. J. et al. McCauley, "Marine defaunation: animal loss in the global ocean," *Science*, vol. 347, 2015.

[4] J. H. Steele, S. A. Thorpe, and K. K. Turekian, *Encyclopedia of Ocean Sciences 2nd Ed.*, Academic Press, 2009.

[5] "The first practical uses of underwater acoustics: The early 1900s," Jul 2017.

[6] Stojanovic M., "Recent advances in high rate underwater acoustic systems," *IEEE J Oceanic Eng.*, vol. 21, pp. 125–136, 1984.

[7] M. Stojanovic and J. Preisig, "Underwater acoustic communication channels: Propagation models and statistical characterization," *IEEE Communications Magazine*, vol. 47, no. 1, pp. 84–89, January 2009.

[8] Linglong Dai, Zhaocheng Wang, Jun Wang, and Zhixing Yang, "Joint Time-Frequency Channel Estimation for Time Domain Synchronous OFDM Systems," *IEEE Transactions on Broadcasting*, vol. 59, no. 1, pp. 168–173, 2013.

[9] Yifan Zhang, Jinhua Wang, Yaqing Huang, and Zhigang Gao, "A Cooperative Approach for Adaptive Channel Discovery in Underwater Acoustic Communication," *Sensors*, vol. 20, no. 7, pp. 2012, 2020.

[10] Liang Wang, Yongqiang Yu, Kun Xie, Xuan Zhu, Guangjie Liu, Jiafeng Wang, and Hongming Zhang, "Accurate Channel Estimation and Adaptive Underwater Acoustic Communications Based on Gaussian Likelihood and Constellation Aggregation," *Sensors (Basel, Switzerland)*, vol. 22, no. 6, pp. 2142–, 2022.

[11] Koen C.H. Blom, Henry S. Dol, Frank Berning, and Paul A. Van Walree, "Development of a Physical Layer for Adaptive Underwater Acoustic Communications," in *2022 Sixth Underwater Communications and Networking Conference (UComms)*, 2022, pp. 1–5.

[12] Stefano Mangione, Giovanni Ettore Galioto, Daniele Croce, Ilenia Tinnirello, and Chiara Petrioli, "A channel-aware adaptive modem for underwater acoustic communications," *IEEE Access*, vol. 9, pp. 76340–76353, 2021.

[13] Emrecan Demirors, George Sklivanitis, G. Enrico Santagati, Tommaso Melodia, and Stella N. Batalama, "A high-rate software-defined underwater acoustic modem with real-time adaptation capabilities," *IEEE Access*, vol. 6, pp. 18602–18615, 2018.

[14] Andreja Radosevic, Rameez Ahmed, Tolga M. Duman, John G. Proakis, and Milica Stojanovic, "Adaptive ofdm modulation for underwater acoustic communications: Design considerations and experimental results," *IEEE Journal of Oceanic Engineering*, vol. 39, no. 2, pp. 357–370, 2014.

[15] Koen C.H. Blom, Henry S. Dol, Frank Berning, and Paul A. Van Walree, "Development of a physical layer for adaptive underwater acoustic communications," in *2022 Sixth Underwater Communications and Networking Conference (UComms)*, 2022, pp. 1–5.

[16] Konstantinos Pelekanakis, Luca Cazzanti, Giovanni Zappa, and João Alves, "Decision tree-based adaptive modulation for underwater acoustic communications," in *2016 IEEE Third Underwater Communications and Networking Conference (UComms)*, 2016, pp. 1–5.

[17] Alex Hamilton, Jack Barnett, and Amy-Mae Hobbs, "Phorcys, an evolution of janus," in *2022 Sixth Underwater Communications and Networking Conference (UComms)*, 2022, pp. 1–4.

[18] J. Potter, J. Alves, D. Green, I. Nissen G. Zappa, and K. McCoy, "The JANUS Underwater Communications Standard," *2014 Underwater Communications and Networking (UComms)*, pp. 1–4, Sept 2014.

[19] S. Blouin, "Preliminary analysis of arctic underwater communication experiments: Summer 2019," 2019.

[20] A. Bhattacharya, J. MacDonald, Jean-François Bousquet, and Stephane Blouin, "On the feasibility of ofdm for long-range mobile communications in the northwest passage," in *2022 Sixth Underwater Communications and Networking Conference (UComms)*, 2022, pp. 1–5.

[21] B. Muquet, Zhengdao Wang, G.B. Giannakis, M. de Courville, and P. Duhamel, "Cyclic prefixing or zero padding for wireless multicarrier transmissions?," *IEEE Trans. Commun.*, vol. 50, no. 12, pp. 2136–2148, 2002.

[22] David Tse and Pramod Viswanath, "Fundamentals of wireless communication," 2005.

[23] M. Stojanovic and J. Preisig, "Underwater acoustic communication channels: Propagation models and statistical characterization," *IEEE Communications Magazine*, vol. 47, no. 1, pp. 84–89, 2009.

[24] Lanjun Liu, Yonglei Zhang, Pengcheng Zhang, Lin Zhou, Jianfen Li, Jiucai Jin, Jie Zhang, and Zhichao Lv, "Pn sequence based doppler and channel estimation for underwater acoustic ofdm communication," in *2016 IEEE International Conference on Signal Processing, Communications and Computing (ICSPCC)*, 2016, pp. 1–6.

[25] Huajian Chen and Chenhao Qi, "Underwater acoustic channel estimation via fast bayesian matching pursuit," in *2017 9th International Conference on Wireless Communications and Signal Processing (WCSP)*, 2017, pp. 1–6.

[26] Guo Long-xiang, Liu Jia-ao, Zhang Xiao, Ge Wei, and Han Xiao, "Robust underwater acoustic channel estimation in impulsive noise environment," in *2021 IEEE/CIC International Conference on Communications in China (ICCC Workshops)*, 2021, pp. 278–281.

[27] Yishan Su, Xuan Liu, Zhigang Jin, and Xiaomei Fu, "Fast estimation of underwater acoustic multipath channel based on lfm signal," in *Global Oceans 2020: Singapore – U.S. Gulf Coast*, 2020, pp. 1–5.

[28] Yuhang Wang, Wei Li, and Zhonghan Hao, "Reinforcement learning-based underwater acoustic channel tracking with forgetting factors," in *OCEANS 2022, Hampton Roads*, 2022, pp. 1–5.

[29] Dennis Sundman, Saikat Chatterjee, and Mikael Skoglund, "A greedy pursuit algorithm for distributed compressed sensing," in *2012 IEEE International Conference on Acoustics, Speech and Signal Processing (ICASSP)*, 2012, pp. 2729–2732.

[30] Weihua Jiang and Roee Diamant, "Sparse channel estimation for long range underwater acoustic communication," in *2022 Sixth Underwater Communications and Networking Conference (UComms)*, 2022, pp. 1–4.

[31] Andrea Petroni, Gaetano Scarano, Roberto Cusani, and Mauro Biagi, "On the effect of channel knowledge in underwater acoustic communications: Estimation, prediction and protocol," *Electronics*, vol. 12, no. 7, 2023.

[32] Joël Trubuil and Thierry Chonavel, "Accurate doppler estimation for underwater acoustic communications," in *2012 Oceans - Yeosu*, 2012, pp. 1–5.

[33] Joël Trubuil, Thierry Le Gall, and Thierry Chonavel, "Synchronization, doppler and channel estimation for ofdm underwater acoustic communications," in *OCEANS 2014 - TAIPEI*, 2014, pp. 1–6.

[34] Yifu Luan, Shefeng Yan, Ye Qin, and Lijun Xu, "Doppler estimation using time reversal mirror for underwater acoustic time-varying multipath channel," in *2017 IEEE International Conference on Signal Processing, Communications and Computing (ICSPCC)*, 2017, pp. 1–9.

[35] J. Alves, T. Furfaro, K. LePage, A. Munafò, K. Pelekanakis, R. Petroccia, and G. Zappa, "Moving janus forward: A look into the future of underwater communications interoperability," in *OCEANS 2016 MTS/IEEE Monterey*, Sep. 2016, pp. 1–6.

[36] Jinfeng Li, Joseph Halt, and Y. Rosa Zheng, "Utilizing janus for very high frequency underwater acoustic modem," in *Global Oceans 2020: Singapore – U.S. Gulf Coast*, 2020, pp. 1–6.

[37] Concetta Baldone, Giovanni Ettore Galioto, Daniele Croce, Ilenia Tinnirello, and Chiara Petrioli, "Doppler estimation and correction for janus underwater communications," in *GLOBECOM 2020 - 2020 IEEE Global Communications Conference*, 2020, pp. 1–6.

[38] M. Stojanovic and P-P J. Beaujean, "Acoustic communication," in *Springer Handbook of Ocean Engineering*, Manhar R. Dhanak and Nikolaos I. Xiros, Eds., pp. 359–386. Springer International Publishing, Cham, 2016.

[39] Habib Mirhedayati Roudsari and Jean-Francois Bousquet, "A Time-Varying Filter for Doppler Compensation Applied to Underwater Acoustic OFDM," *Sensors*, vol. 19, no. 1, 2019.

Appendix A

Copyright Permissions

IEEE COPYRIGHT FORM

To ensure uniformity of treatment among all contributors, other forms may not be substituted for this form, nor may any wording of the form be changed. This form is intended for original material submitted to the IEEE and must accompany any such material in order to be published by the IEEE. Please read the form carefully and keep a copy for your files.

CROWN COPYRIGHT CERTIFICATION AND GRANT OF RIGHTS

This will certify that all authors of the Work are employees of the British or a British Commonwealth Government and prepared the Work in connection with their official duties. As such, the Work is subject to Crown Copyright and is not assigned to the IEEE. However, the undersigned herewith acknowledges that the IEEE is granted an irrevocable, exclusive, royalty-free, non-assignable, worldwide license to adapt, reproduce, print, publish, make derivative works, and make available the Work in any media, whether now known or hereinafter created, including, but not limited to, print, digital, and electronic formats for any lawful purposes. This license shall not modify the ownership of the intellectual property rights contained within the Work (including but not limited to patent, trademark rights and copyright) which shall rest with the British Crown Government.

GENERAL TERMS

1. The undersigned represents that he/she has the power and authority to make and execute this form.
2. The undersigned agrees to indemnify and hold harmless the IEEE from any damage or expense that may arise in the event of a breach of any of the warranties set forth above.
3. The undersigned agrees that publication with IEEE is subject to the policies and procedures of the IEEE PSPB Operations Manual.
4. In the event the above work is not accepted and published by the IEEE or is withdrawn by the author(s) before acceptance by the IEEE, the foregoing copyright transfer shall be null and void. In this case, IEEE will retain a copy of the manuscript for internal administrative/record-keeping purposes.
5. For jointly authored Works, all joint authors should sign, or one of the authors should sign as authorized agent for the others.
6. The author hereby warrants that the Work and Presentation (collectively, the "Materials") are original and that he/she is the author of the Materials. To the extent the Materials incorporate text passages, figures, data or other material from the works of others, the author has obtained any necessary permissions. Where necessary, the author has obtained all third party permissions and consents to grant the license above and has provided copies of such permissions and consents to IEEE

You have indicated that you DO NOT wish to have video/audio recordings made of your conference presentation under terms and conditions set forth in "Consent and Release."

BY TYPING IN YOUR FULL NAME BELOW AND CLICKING THE SUBMIT BUTTON, YOU CERTIFY THAT SUCH ACTION CONSTITUTES YOUR ELECTRONIC SIGNATURE TO THIS FORM IN ACCORDANCE WITH UNITED STATES LAW, WHICH AUTHORIZES ELECTRONIC SIGNATURE BY AUTHENTICATED REQUEST FROM A USER OVER THE INTERNET AS A VALID SUBSTITUTE FOR A WRITTEN SIGNATURE.

Michel DuCharme PhD EiC for DRDC	13-07-2022
Signature	**Date (dd-mm-yyyy)**

Information for Authors

AUTHOR RESPONSIBILITIES

The IEEE distributes its technical publications throughout the world and wants to ensure that the material submitted to its publications is properly available to the readership of those publications. Authors must ensure that their Work meets the

requirements as stated in section 8.2.1 of the IEEE PSPB Operations Manual, including provisions covering originality, authorship, author responsibilities and author misconduct. More information on IEEE's publishing policies may be found at http://www.ieee.org/publications_standards/publications/rights/authorrightsresponsibilities.html Authors are advised especially of IEEE PSPB Operations Manual section 8.2.1.B12: "It is the responsibility of the authors, not the IEEE, to determine whether disclosure of their material requires the prior consent of other parties and, if so, to obtain it." Authors are also advised of IEEE PSPB Operations Manual section 8.1.1B: "Statements and opinions given in work published by the IEEE are the expression of the authors."

RETAINED RIGHTS/TERMS AND CONDITIONS

- Authors/employers retain all proprietary rights in any process, procedure, or article of manufacture described in the Work.
- Authors/employers may reproduce or authorize others to reproduce the Work, material extracted verbatim from the Work, or derivative works for the author's personal use or for company use, provided that the source and the IEEE copyright notice are indicated, the copies are not used in any way that implies IEEE endorsement of a product or service of any employer, and the copies themselves are not offered for sale.
- Although authors are permitted to re-use all or portions of the Work in other works, this does not include granting third-party requests for reprinting, republishing, or other types of re-use.The IEEE Intellectual Property Rights office must handle all such third-party requests.
- Authors whose work was performed under a grant from a government funding agency are free to fulfill any deposit mandates from that funding agency.

AUTHOR ONLINE USE

- **Personal Servers**. Authors and/or their employers shall have the right to post the accepted version of IEEE-copyrighted articles on their own personal servers or the servers of their institutions or employers without permission from IEEE, provided that the posted version includes a prominently displayed IEEE copyright notice and, when published, a full citation to the original IEEE publication, including a link to the article abstract in IEEE Xplore. Authors shall not post the final, published versions of their papers.
- **Classroom or Internal Training Use.** An author is expressly permitted to post any portion of the accepted version of his/her own IEEE-copyrighted articles on the author's personal web site or the servers of the author's institution or company in connection with the author's teaching, training, or work responsibilities, provided that the appropriate copyright, credit, and reuse notices appear prominently with the posted material. Examples of permitted uses are lecture materials, course packs, e-reserves, conference presentations, or in-house training courses.
- **Electronic Preprints.** Before submitting an article to an IEEE publication, authors frequently post their manuscripts to their own web site, their employer's site, or to another server that invites constructive comment from colleagues. Upon submission of an article to IEEE, an author is required to transfer copyright in the article to IEEE, and the author must update any previously posted version of the article with a prominently displayed IEEE copyright notice. Upon publication of an article by the IEEE, the author must replace any previously posted electronic versions of the article with either (1) the full citation to the IEEE work with a Digital Object Identifier (DOI) or link to the article abstract in IEEE Xplore, or (2) the accepted version only (not the IEEE-published version), including the IEEE copyright notice and full citation, with a link to the final, published article in IEEE Xplore.

Questions about the submission of the form or manuscript must be sent to the publication's editor.
Please direct all questions about IEEE copyright policy to:
IEEE Intellectual Property Rights Office, copyrights@ieee.org, +1-732-562-3966

DATA TRANSFER AGREEMENT (DTA)
& NON-DISCLOSURE AGREEMENT

BETWEEN:

HIS MAJESTY THE KING IN RIGHT OF CANADA, acting through and represented by the Minister of the Department of National Defence (DND), as further represented by Defence Research and Development Canada (DRDC), having its headquarters at 60 Moodie Drive, Ottawa, Ontario, K1A 0K2.

Hereinafter referred to as the "Crown"

AND

10945773 Canada Inc, a non-for-profit private company registered in Nova Scotia, having its headquarters at 23 Albion Rd, Halifax, Nova Scotia, Canada B3P 1P8, Canada.

Hereinafter referred to as the"Recipient"

The Crown and the Recipient are jointly referred to as the "Parties" and individually as a "Party".

WHEREAS the Recipient has requested the transfer of certain proprietary Data of the Crown. The Crown has agreed to transfer the Data to the Recipient for the Purpose of evaluating, conducting feasibility testing, and improving the performance of long-range and robust underwater acoustic communication protocols in supportof the DRDC's Defense of North America (DNA) program;

WHEREAS the Parties wish to enter into discussions to evaluate their mutual interest in pursuing a collaboration related to long-range and robust underwater acoustic communication protocols in support of the DRDC's Defense of North America (DNA) program, (hereinafter referred to as the "**the Purpose**"), under the provisions of this Agreement**;**

NOW THEREFORE, in consideration of the mutual benefits derived from said transfer, the Parties agree that any such data transfer shall be governed as follows:

1. DEFINITIONS

In this Agreement, the following term shall have the respective following meaning:

"**Effective Date**" means the date that the last Party becomes signatory to this Agreement, or until such other time as may be established in writing in a further, or substitute arrangement between the Parties.

2. CONDITIONS

2.1. The Crown will provide to the Recipient for use only for the Purpose, by its Technical Authority, the following data, as detailed herein or in Appendix A of this Agreement (hereinafter referred to as the "**Data**"):

A data set acquired by DRDC during an experiment conducted in the summers of 2019 and 2023. These Data are UNCLASSIFIED and comprise acoustic recordings of transmitted signals (original signal developed by the Recipient), a set of non- acoustic data files and measurements made to capture the experimental context, drawing files,documents about instruments specifications, scripts to read files, and other supporting documents.

For the purpose of this Agreement, the Recipient's Technical Authority will be Dr. Michel Barbeau.

2.2. "**Confidential Information**" means the information identified in Annex A or other information related to the Purpose provided by one Party to the other Party during the Term, which is clearly marked "CONFIDENTIAL," or if related orally or visually, identified as "CONFIDENTIAL" at the time of disclosure. These Data will not be used, transferred, distributed, released or disclosed by the Technical Authority or the Recipient in whole or in part to any other person, except to those individuals working under the Technical Authority or his/her successors' direct supervision. It will be used only in facilities of the Recipient and will not be taken to any other location, unless specificallyprescribed in the Purpose or by prior written permission obtained from the Crown. The Recipient will use its best efforts to treat and keep confidential, and cause its officers, employees, and contractors to keep confidential any such information received by it from the Crown for use by the Recipient for the Purpose. Notwithstanding this clause, the Recipient may disclose the information identified in Annex A to employees who need to know such information in order to perform work related to the Purpose; provided that each such person has a legal or contractual obligation to maintain the confidentiality of such information.

The above restrictions on disclosure shall not apply to information which:

a. is in the Recipient's possession before receipt thereof under this Agreement, as evidenced by its written records; or
b. is disclosed or provided to the Recipient by a third party without a duty of confidentiality; or
c. is or becomes part of the public domain through no fault of the Recipient; or
d. has been independently evaluated and developed by the Recipient prior to disclosure, as evidenced by its written records; or
e. is made in accordance with legislation or a lawful order of a court or administrative tribunal requiring the Recipient to disclose any or all of the information, provided the Recipient shall promptly notify the Crown allowing some reasonable time to oppose such process, before disclosure occurs.

2.3. The Parties agree that the classification of these Data is UNCLASSIFIED.

2.4. These Data will be used within the confines of the Purpose only, within the appropriate network and repository (as per its classification level) and will not be used for consulting, licensing, or other contractual arrangements with any third party unless a license is obtained from the Crown.

2.5. These Data shall be used in compliance with all applicable laws, regulations, policies and guidelines.

2.6. The Recipient agrees to ensure that anyone who has access to these Data complies with the terms of this DTA.

2.7. Not publish the results of its studies performed with these Data or any of the Data itself, without prior written consent from the Crown.

3. REPRESENTATIONS, WARRANTIES AND INDEMNIFICATION

3.1. The Data is provided "as is", and the Crown makes no express or implied warranties of merchantability or fitness of the Data for a particular purpose. Within the scope of the Purpose, the Crown shall not be liable for any claims arising out of or connected with the useof the Data. Furthermore, the Crown makes no representation that the use of the Data is not infringing or will not infringe any patents or proprietary rights of third parties.

3.2. The Recipient agrees that it will indemnify and save harmless the Crown from and against all claims, demands, losses, damages, costs (including reasonable solicitor and client costs), actions, suits or proceedings brought by a third party, that are in any manner arising out of, related to, occasioned by, or attributed to the use of said Data, except that Recipient will not be required to indemnify an Indemnitee to the extent such liabilities, claims, damages, losses or expenses are caused by the gross negligence or willful misconduct of that Indemnitee and/or use of the results.

4. GENERAL

4.1. This Agreement may be executed in counterparts, each of which shall be deemed to be an original as against any Party whose signatures appears thereon, and all of which shall together constitute one and the same instrument. This Agreement shall become binding whenone or more counterparts hereof, individually or taken together, shall bear the signatures of all the Parties reflected herein as the signatories. Signatures transmitted by electronic signature shall be acceptable to bind each Party and shall not affect the validity of this Agreement in any way.

4.2. This Agreement shall be governed and interpreted in accordance with the laws in effect inthe Province of Nova Scotia.

5. TERM AND TERMINATION

5.1. This Agreement shall be effective as of the date the last Party becomes signatory to this Agreement ("**Effective Date"**) and shall expire on the earlier of **twenty-four (24) months** after the Effective Date, or upon termination of this Agreement. However, all obligations of confidence, restrictions and non-use created, shall remain in force for **five (5) years** from the expiry or termination of this Agreement.

5.2. This Agreement may be terminated immediately by the Crown upon the Recipient's breachof any its terms and conditions.

5.3. This Agreement may be terminated by mutual agreement at any time and, if mutual agreement cannot be reached, this Agreement may be terminated by either Party upon **ninety (90) days** written notice.

5.4. Upon termination or expiry of this Agreement, the Recipient shall make no further use of the Data. The Crown shall instruct the Recipient the manner in which said Data is to be destroyed or returned to the Crown. The Recipient shall provide a written notification to the Crown that it has returned or destroyed all whole or partial copies of said Data, in all formats, and has deleted the Data from all databases and other electronic repositories within its possession, as instructed by the Crown.

5.5. Any demand, notice or other communication to be given in connection with this agreement shall be given in writing and shall be given by personal delivery, by registered mail or email addressed to Recipient as follows:

If to the Crown:
Etienne Dubois
Deputy Director External Partnerships and Engagements
Atlantic Research Centre
9 Grove Street
Dartmouth, NS
B2Y 3Z7
Email:Etienne.dubois2@forces.gc.ca

If to the Recipient:

For Contractual Matters:
Dr. Jean-Francois Bouquet, PhD, Peng.
10945773 Canada Inc.
23 Albion Rd, Halifax,
Nova Scotia, Canada B3P 1P8
Email: jbousquet@dal.ca

IN WITNESS WHEREOF, the Parties hereto have executed this Agreement in duplicate by their proper officers, duly authorized to act on their behalf.

For the Crown:

[redacted]

Warren Connors
Section Head, Under Water Warfare
DRDC – Atlantic Research Centre

[redacted]

Etienne Dubois
Deputy Director External
Engagements and Partnerships
DRDC – Atlantic Research Centre

For the Recipient:

[redacted]

I have authority to bind the Recipient

Jean-Francois Bousquet

Date: 10/31/2023

[redacted]

Annex A

DOCUMENTATION AND ACCEPTANCEOF DATA

The following is a description of the Data, related to the Purpose which the Crown has transferredto the Recipient. Note that this information is UNCLASSIFIED and not Controlled Goods.

1. Data collected by DRDC in the Canadian Arctic during the summers of 2019 and 2023.
2. Acoustic data (time series) of recorded signals and ambient noise on a hydrophone array.
3. Environmental data (sound speed profile, etc.) and other instruments/sensors data (depth,temperature, etc.)
4. Scripts to retrieve data from instruments present at experiment.
5. Particulars of the experiment hydrophone arrangement (drawings, etc.).